(12) LEVEL II

DNA 5451F

AD A105127

ANALYSIS AND MODELING OF PIEZORESISTANCE RESPONSE

Y. M. Gupta

SRI International
333 Ravenswood Avenue
Menlo Park, California 94025

DTIC
ELECTE
OCT 6 1981
S
B

30 September 1980

Final Report for Period 1 April 1979—30 June 1980

CONTRACT No. DNA 001-79-C-0180

DTIC FILE COPY

Prepared for

Director

DEFENSE NUCLEAR AGENCY

Washington, D. C. 20305

UNCLASSIFIED

REPORT DOCUMENTATION PAGE	READ INSTRUCTIONS BEFORE COMPLETING FORM

1. REPORT NUMBER	2. GOVT ACCESSION NO.	3. RECIPIENT'S CATALOG NUMBER
DNA 5451F	AD-A105 127	

4. TITLE (and Subtitle)	5. TYPE OF REPORT & PERIOD COVERED
ANALYSIS AND MODELING OF PIEZORESISTANCE RESPONSE	Final Report for Period 1 Apr 79—30 Jun 80
	6. PERFORMING ORG. REPORT NUMBER
	PYU 8324

7. AUTHOR(s)	8. CONTRACT OR GRANT NUMBER(s)
Y. M. Gupta	
Contributors: D. D. Keough and G. E. Duvall	DNA 001-79-C-0180

9. PERFORMING ORGANIZATION NAME AND ADDRESS	10. PROGRAM ELEMENT PROJECT, TASK AREA & WORK UNIT NUMBERS
SRI International 333 Ravenswood Avenue Menlo Park, California 94025	Subtask J11AAXSX352-61

11. CONTROLLING OFFICE NAME AND ADDRESS	12. REPORT DATE
Director Defense Nuclear Agency Washington, D.C. 20305	30 September 1980
	13. NUMBER OF PAGES
	102

14. MONITORING AGENCY NAME & ADDRESS(if different from Controlling Office)	15. SECURITY CLASS. (of this report)
	UNCLASSIFIED
	15a. DECLASSIFICATION DOWNGRADING SCHEDULE

16. DISTRIBUTION STATEMENT (of this Report)

Approved for public release; distribution unlimited.

17. DISTRIBUTION STATEMENT (of the abstract entered in Block 20, if different from Report)

19. KEY WORDS (Continue on reverse side if necessary and identify by block number)

Stress measurements	Elastic-plastic inclusion
Piezoresistance	Piezoresistive
Wave propagation	Transducers
Dynamic response	

20. ABSTRACT (Continue on reverse side if necessary and identify by block number)

A phenomenological model of piezoresistance was formulated to calculate the resistance change of a gage element subjected to mechanical deformation. This model incorporates the tensor nature of piezoresistivity, elastic-plastic gage response to include mechanical and electrical hysteresis, and dimensional contributions.

The phenomenological model was used to analyze past data on Manganin and ytterbium. The stresses and strains in the gage element, needed for

DD FORM 1473 1 JAN 73   EDITION OF 1 NOV 65 IS OBSOLETE   UNCLASSIFIED

20. Abstract (Continued)

this analysis, were approximated from geometrical considerations. The
results showed that the piezoresistance model was necessary to under-
stand the gage response. However, many experimental results could not
be adequately modeled. Improved analysis requires a rigorous determina-
tion of the stresses and strains in the gage element.

A few well-defined experiments in support of the analysis, were
performed to determine the effect of matrix stress rotation, gage strain
states, and shear loading on gage response. The matrix stress rotation
experiments gave definitive results and showed that the gage response was
governed mainly by the matrix stress component normal to the foil. To
understand these results, it is necessary to determine the gage stresses
and strains.

To rigorously model the gage response, the gage element was repre-
sented as an inclusion and the corresponding boundary value problem was
solved. The Eshelby method for elastic inclusions was modified to
include an elastic-plastic inclusion and to obtain solutions for loading
and unloading. This procedure gave good agreement with experimental data.
Thus, the elastic-plastic inclusion formulation in conjunction with the
phenomenological model can explain piezoresistance response.

SUMMARY

Piezoresistance stress gages have been extensively used for measuring dynamic stresses both in laboratory and field applications. A review of the past work shows that these gages, because of their adaptability to a wide range of stresses and times and their survivability in severe environments, provide a unique measuring system. However, the interpretation of the data for loading conditions deviating significantly from the laboratory calibration experiments is questionable. Also, the gage response in laboratory calibration experiments is not well understood. The goal of this research effort was to develop an improved understanding of piezoresistance gages and to model their response to applied loads to permit improved stress measurements. The work focused on analytic developments, with a few experiments performed in support of the analysis. Specific attention was given to the mechanical interaction between the gage and the matrix.

First, a phenomenological model was formulated to calculate the resistance change of a gage element subjected to mechanical deformation. This formulation incorporates the tensor nature of piezoresistivity, elastic-plastic response of the gage to include mechanical and electrical hysteresis, and dimensional changes. The resistance change expression derived herein is markedly different from the empirical relationship currently used to interpret gage data. This expression points out the importance of knowing the strain states in the gage element and the material constants for the gage. The difficulty of inverting the gage data to determine a particular matrix stress component is also indicated.

Second, past laboratory shock wave data on Manganin and ytterbium were analyzed in terms of the phenomenological model. The stresses and strains in the gage element, needed for this analysis, were approximated using an approach similar to that of Barsis et al. (Ref. 17). For analysis of these data, the normal stress was assumed to be the same as in the matrix and strain states were assumed to be either one-or

1

two-dimensional. The results showed that the phenomenological model was necessary for understanding the piezoresistance response under shock loading and for reconciling shock data with data from other loading conditions. The importance of gage plasticity in modeling the gage response was demonstrated. There are, however, many aspects of the experimental results that cannot be explained by the approximate analysis: Manganin data for a wire and a foil (with similar hydrostatic response) cannot be explained by a single set of parameters, hysteresis corrections cannot be easily incorporated, and the role of matrix stresses and strains on the gage response cannot be determined. These difficulties have pointed out the need for rigorously determining the stresses and strains in the gage element, and the material constants required in the phenomenological model.

Third, a few experiments were performed on ytterbium to examine the role of some important mechanical variables, and to provide data for the subsequent gage-matrix interaction analysis. These experiments examined the effect of (1) rotation of matrix stresses, (2) varying the strain states, and (3) shear loading on the gage response. The latter two set of experiments revealed some interesting results, but they are inconclusive because of lack of experimental reproducibility. The effect of shear loading should be reexamined in future work. The matrix stress rotation experiments showed that the gage response is governed mainly by the stress component normal to the major surface of the foil. These data showed that gage calibrations for one gage orientation with respect to the matrix stress field cannot be applied to another orientation. Also, the results for the rotated orientation (rotated through 90° from the usual orientation) could not be analyzed because the foil stresses and strains in this case could not be easily related to the matrix stress or approximated from simple geometrical constraints.

Finally, to rigorously determine the stresses and strains in the gage foil, the foil was modeled as an inclusion in the matrix and then the corresponding boundary value problem was solved. The foil was modeled as an elliptical inclusion and Eshelby's technique (Ref. 48) for elastic elliptical inclusions was used to determine the stresses and strains.

2

The results of the matrix stress rotation experiments were selected to check the analytic solution. The results showed that the elastic inclusion solution was not appropriate for modeling the gage response. Hence, the Eshelby method was modified to include an elastic-plastic inclusion and to obtain solutions for loading and unloading. This procedure gave good agreement with the data. Thus, the main result of this work is that the elastic-plastic inclusion solution in conjunction with the phenomenological model can explain the response of piezoresistance gages to mechanical loading. The gage-matrix interaction analysis rigorously shows why the gage response in the usual shock wave experiments is dominated by the normal stress as assumed in the empirical relationship. The theoretical solutions show many interesting features during the elastic-plastic transition and upon unloading, and should be compared with experimental results over a wide range of stresses. Effect of the foil aspect ratio can also be determined with this analysis.

In conclusion, the objectives of the present study were successfully completed. The response of piezoresistance gages to mechanical loads can now be explained and modeled with a phenomenological model. However, further work is needed to determine the material constants for the model, to quantitatively account for gage hysteresis, and to quantitatively confirm the present work over a wider range of loading conditions. Specific recommendations for using piezoresistance gages in complex loading situations are presented.

Accession For

NTIS CRA&I
DTIC TAB
Unannounced
Justification

By
Distribution/
Availability Codes
Avail and/or
Dist   Special

A

3

PREFACE

Conversion factors for U.S. customary to metric (SI) units of measurement.

To Convert From	To	Multiply By
angstrom	meters (m)	1.000 000 X E -10
atmosphere (normal)	kilo pascal (kPa)	1.013 25 X E +2
bar	kilo pascal (kPa)	1.000 000 X E +2
barn	meter² (m²)	1.000 000 X E -28
British thermal unit (thermochemical)	joule (J)	1.054 350 X E +3
cal (thermochemical)/cm²§	mega joule/m² (MJ/m²)	4.184 000 X E -2
calorie (thermochemical)§	joule (J)	4.184 000
calorie (thermochemical)/g§	joule per kilogram (J/kg)*	4.184 000 X E +3
curie§	giga becquerel (GBq)†	3.700 000 X E +1
degree Celsius‡	degree kelvin (K)	$t_K = t^\circ_C + 273.15$
degree (angle)	radian (rad)	1.745 329 X E -2
degree Fahrenheit	degree kelvin (K)	$t_K = (t^\circ_F + 459.67)/1.8$
electron volt§	joule (J)	1.602 19 X E -19
erg§	joule (J)	1.000 000 X E -7
erg/second	watt (W)	1.000 000 X E -7
foot	meter (m)	3.048 000 X E -1
foot-pound-force	joule (J)	1.355 818
gallon (U.S. liquid)	meter³ (m³)	3.785 412 X E -3
inch	meter (m)	2.540 000 X E -2
jerk	joule (J)	1.000 000 X E +9
joule/kilogram (J/kg) (radiation dose absorbed)§	gray (Gy)*	1.000 000
kilotons§	terajoules	4.183
kip (1000 lbf)	newton (N)	4.448 222 X E +3
kip/inch² (ksi)	kilo pascal (kPa)	6.894 757 X E +3
ktap	newton-second/m² (N·s/m²)	1.000 000 X E +2
micron	meter (m)	1.000 000 X E -6
mil	meter (m)	2.540 000 X E -5
mile (international)	meter (m)	1.609 344 X E +3
ounce	kilogram (kg)	2.834 952 X E -2
pound-force (lbf avoirdupois)	newton (N)	4.448 222
pound-force inch	newton-meter (N·m)	1.129 848 X E -1
pound-force/inch	newton/meter (N/m)	1.751 268 X E +2
pound-force/foot²	kilo pascal (kPa)	4.788 026 X E -2
pound-force/inch² (psi)	kilo pascal (kPa)	6.894 757
pound mass (lbm avoirdupois)	kilogram (kg)	4.535 924 X E -1
pound mass-foot² (moment of inertia)	kilogram-meter² (kg·m²)	4.214 011 X E -2
pound mass/foot³	kilogram/meter³ (kg/m³)	1.601 846 X E +1
rad (radiation dose absorbed)§	gray (Gy)*	1.000 000 X E -2
roentgen§	coulomb/kilogram (C/kg)	2.579 760 X E -4
shake	second (s)	1.000 000 X E -8
slug	kilogram (kg)	1.459 390 X E +1
torr (mm Hg, 0° C)	kilo pascal (kPa)	1.333 22 X E -1

*The gray (Gy) is the accepted SI unit equivalent to the energy imparted by ionizing radiation to a mass of energy corresponding to one joule/kilogram.
†The becquerel (Bq) is the SI unit of radioactivity. 1 Bq = 1 event/s.
‡Temperature may be reported in degree Celsius as well as degree kelvin.
§These units should not be converted in DNA technical reports; however, a parenthetical conversion is permitted at the author's discretion.

5

TABLE OF CONTENTS

7

LIST OF TABLES

8

SECTION 1

1.1 MOTIVATION AND OBJECTIVES

Characterization of dynamic stresses/loads in geologic media and around structures is an important and continuing requirement for DNA programs both in laboratory and field applications.[1-3] Ascertaining material and structural response, improved development of material models, and verification of code calculations require reliable stress measurements. Because of their adaptibility and survivability, piezoresistance gages are used extensively for stress measuremnts.[4] These gages are unique because of the stress range (1 MPa-100 GPa) and time range (20 ns-static loading) over which they can be used.[5] Gage usage is based on an empirical relationship between the resistance change and one stress component obtained from a laboratory calibration experiment along a particular loading path (uniaxial strain). However, detailed examination of the theoretical relationship between the resistance change and mechanical loading (discussed in Sections 1.2 and 2) shows that piezoresistance gage response is more complex and depends on several variables; therefore the current interpretation of gage data for loading conditions deviating significantly from the laboratory calibration is questionable. Cross-checking with other gage types and/or numerical calculations is not satisfactory because these results are themselves prone to error (particularly in field data). To increase confidence in the use of piezoresistance gages and to develop better gage packages, we need to develop a more fundamental understanding of piezoresistance gage response. Specifically, this approach is needed to determine the accuracy in using these gages, in resolving differences between field data, and in making better stress measurements under conditions of interest.

The goal of the present work was to attain an improved understanding of piezoresistance gage measurements by performing well-defined analyses and laboratory experiments. An important aspect of the present work was to focus attention on the mechanical interaction of the gage with its surroundings. This problem, though useful for all gage types,

has received little attention in previous studies. Some specific objectives of our work were as follows:

- Develop a phenomenological model for piezoresistance to calculate resistance change under mechanical loading. Review the literature and analyze the past data in terms of this model.

- Experimentally determine the role of matrix stresses, shear deformation, and strain states in the gage on the gage response.

- Develop a theoretical analysis to examine the mechanical interaction between the gage and the matrix material.

1.2 BACKGROUND

In this subsection we briefly discuss piezoresistance gage usage, review the past work, and summarize the findings. Instead of presenting a chronological review of the past work, we discuss related previous studies in analyzing the working of a piezoresistance gage. Hence, not every paper on the subject that is known to us is included in the discussion. However, the literature cited is sufficiently comprehensive to provide a good state-of-the-art review.

The resistance of a conductor can be written as

$$R = \frac{\rho \cdot \ell}{A} \tag{1.1}$$

where ρ is the resistivity, ℓ is the length, and A is the area of cross-section normal to the length ℓ. The vector nature of R and the tensor nature of ρ have been intentionally suppressed for the present. The conceptual basis for using piezoresistance gages to measure stress is based on relating the change in resistivity (ρ) of the gage to applied stresses. We emphasize, for later discussion, that the experimental measurements consist of measuring resistance (R) and not resistivity (ρ) changes.[*] Therefore, the term 'piezoresistance' is more appropriate than 'piezoresistive' to denote these gages.

---

[*]The inability to directly measure resistivity causes many of the difficulties in complex loading situations.

The use of piezoresistance gages dates back to the high pressure work of Bridgeman and others at the turn of the century.[6] Bridgeman was also the first to formulate the tensor nature of piezoresistance measurements.[7] Since then, these gages have been used routinely in high pressure studies to monitor hydrostatic pressure.[8] In addition, an understanding of piezoresistive phenomenon, particularly in semi-conductors, in terms of the band structure of solids has been an area of interest to solid state physicists.[9,10] Because the present work is concerned with gage response for application to stress measurements, we will use a purely continuum approach in our discussion.

The first attempts to develop piezoresistance transducers for dynamic loading* appear to be those of Hauver,[11] who measured resistance changes in shocked sulphur. Subsequently, in 1964, Fuller and Price, and Bernstein and Keough reported piezoresistance measurements for Manganin wires under shock loading.[12,13] In these and subsequent studies, the principle for using these gages can be summarized as follows: In a calibration experiment, the resistance change of an element (contained) in a matrix is measured as a function of a specific stress component in the matrix.† By repeating the measurements for several stresses, we can write the following empirical relationship

$$\frac{\Delta R}{R_o} = K \cdot \sigma_n \qquad (1.2)$$

where ΔR = change in resistance

R_o = original resistance

σ_n = peak longitudinal stress in the matrix

K = empirically determined constant that is generally a function of σ_n.

---

*The development of piezoresistance transducers for dynamic loading was a direct outgrowth of the high pressure work.

†Most calibration data are based on shock wave uniaxial strain experiments and the stress component is the longitudinal or normal stress component. Note, uniaxial strain refers to the state of strain in the matrix.

Once K has been determined, the gage measurement from an experiment of interest can be used to determine σ_n by inverting Equation (1.2).

We point out that the use of piezoresistance gages in shock loading is assumed to involve no stress wave phenomenon. The gage is like a static probe that can respond rapidly to the stress states around it. The differences between gage response under hydrostatic loading and shock wave loading occur because of differences in the mechanical state of the gage in the two cases.

Since 1964, many papers have been published on calibration of piezoresistance gages. Most of the work has been on Manganin[14-19] (nominal composition 84% Cu, 12% Mn, and 4% Ni) with a few studies on ytterbium.[20,21] Manganin, in contrast to ytterbium, has the advantages that its resistivity is relatively insensitive to temperature, the batch-to-batch material variability can be better controlled, and the response is nearly linear (constant K) over a wide stress range. Ytterbium gages have been primarily developed in the last 5 to 10 years and their principle advantage over Manganin is their greater sensitivity to stress.[*] Therefore, Yb gages are preferable in the range 10 MPa-2.0 GPa. (The upper limit for using Yb is 3.0 GPa.) For stresses above 2.0 GPa, the resistivity changes in Manganin are sufficiently large and the use of Manganin is preferable because of the other advantages cited above.

Under dynamic loading the most common usage of piezoresistance gages has been in measuring longitudinal stress in shock wave uniaxial strain experiments in the 1 to 20 GPa range. Even for this particular

[*] Because of its low atomic weight, carbon is often used in stress measurements in radiation deposition studies. Recently, these gages have been used in conventional shock studies.[22-24] In our work, we focus on Manganin and ytterbium because these are most commonly used. Other materials that have been considered, but not pursued, as piezoresistance gages are Li and Ca.[25]

loading configuration, many different calibration studies (determination of K versus σ_n) have been reported. These studies have largely been prompted by the need to calibrate the specific gage material and grid configuration being used in a particular series of experiments. The lack of a universal calibration (or a standard gage type) in prior work is inefficient, but does not pose a conceptual difficulty in gage usage for uniaxial strain experiments.

In recent years, there has been a growing interest in extending the use of piezoresistance gages to loading conditions far removed from the hydrostatic high pressure and/or the shock wave uniaxial strain configurations. This is particularly true for DNA field applications and armor penetration studies. Unfortunately, extrapolating the gage response (or calibration) to new loading conditions may not be simple. The empirical procedure indicated by Equation (1.2) and discussed earlier is satisfactory if the gage is used in a loading situation that closely matches the calibration conditions. When the two do not match, the empirical calibration studies are of limited use in extrapolating the gage response. Because of the lack of an alternative, the uniaxial strain calibration is commonly used for other loading situations (e.g., divergent flow). In the following paragraphs we discuss the factors that make it difficult to apply uniaxial strain calibration to more general loading conditions and to invert the gage data under arbitrary loading.*

The calibration experiments measure resistance change and not resistivity; thus resistivity and dimensional changes cannot be easily separated. If, in the experiment of interest, the dimensional changes are significantly different from the calibration experiments, then it is difficult to account for them. One potential solution that has been suggested is to use a nonpiezoresistive material to obtain a measure of purely dimensional changes in the experiment of interest.[26] This is an interesting concept that needs to be further examined theoretically and in well-defined experiments. This concept is discussed further in Section 2.3.

---

*Some of the discussion presented here uses concepts that are described in Section 2.

The function relating resistivity changes and stress, in general, is not a scalar but a fourth-rank tensor.[27] For isotropic materials (wich describe all the polycrystalline materials of interest), there are two independent constants similar to Lame's constants in elasticity. Also, for applications to high stresses the nonlinear form of these constants needs to be included. Without a knowledge of the complete set of constants, it is not possible to invert the resistivity measurements to determine the corresponding stresses. In fact, the tensor nature of piezoresistivity raises the question: Is the response related uniquely to only one stress component as is commonly assumed? This question is considered in detail in this report.

The gage undergoes plastic deformation, which results in residual resistance as is commonly observed in shock wave uniaxial strain data. The hypothesis that this residual resistance is caused by the production of lattice defects (the change in the stress-free resistivity) is supported by studies on annealed and cold-rolled Manganin[28] and Silver[29] foils. In Sections 2 and 3, we discuss another contribution to residual resistance: mechanical hysteresis. This phenomenon, expected to be important at low stress levels, has not been considered in previous studies. Grady and Ginsberg reconciled their shock data on Yb with the hydrostatic data by subtracting the resistance that remained after unloading from the peak value.[30] Steinberg and Banner proposed an ad-hoc method to account for resistance hysteresis by using a different calibration for loading and unloading.[31] More recently, Vantine et. al., on the basis of a large number of experiments in Manganin, have presented an empirical approach to account for the hysteresis.[32] They present a single relation for use during loading and unloading. The difficulty with these approaches is similar to that in using Equation (1.2). As long as the use of the gage is similar to the calibration conditions, the correction may be adequate. However, for loading conditions that deviate from the calibration conditions, the procedure will lead to errors. The magnitude of these errors depends on the loading conditions in a particular application. A more fundamental approach is needed to account for hysteresis corrections.

14

Finally, there is the question of gage-matrix mechanical interaction. (In actual usage the gage is generally contained in a thin film of epoxy.) There are two main contributing factors: the gage shape and the difference between the mechanical properties of the gage and the matrix. Calibration studies on wires and foils with similar hydrostatic response give different results under shock loading, demonstrating that the shape (or at least large differences in the aspect ratio) can make a difference.[16] We point out that most experiments are now done with foils. Whether small differences in aspect ratio can make a large difference in calibration is not known.

Except for two papers,[17,30] the subject of actual strain states in the gage foils has not been considered in past work. Even in these two studies, simple strain states were assumed, as discussed in detail in Section 3. There have also been attempts to vary the matrix material and examine the gage response in uniaxial strain loading.[16] The results are inconclusive because of large scatter in the data. Although the gage-matrix interaction problem can be neglected for uniaxial strain applications with thin foils* (because the calibration data are for similar conditions), it may be very important for using a gage calibration from one loading situation to a different loading situation. Our examination of existing papers shows a general lack of gage-matrix interaction studies in the use of piezoresistance gages. We point out that in field applications, there is an additional metallic encapsulation to facilitate handling and to improve gage survival. In such situations the gage-matrix interaction must include the influence of the metallic encapsulation.

Clearly, the response of piezoresistance gages to mechanical loads is complicated. Although we have attempted to separate these complexities, for an actual experimental situation they are coupled, making the inversion of the gage data difficult. In fact, it can be questioned whether these gages can ever be used with a high degree of accuracy in testing situations that deviate significantly from the calibration loading conditions. Before taking such a pessimistic position, it is important to examine the reasons for using these gages and to review the experimental work.

---

*This is demonstrated rigorously later in this report.

The main reason for using these gages is their versatility and the general lack of suitable alternative methods for stress measurements. Although piezoelectric or diaphragm (strain gages) gages can be used for a specific situation, they are far too restrictive compared to piezoresistance gages.[2] Studies[5,19] at SRI have shown that with special care, piezoresistance gages can be used for stresses as low as 1 MPa and as high as 100 GPa. The lower limit is with Yb gages and the upper limit is with Manganin gages. No other gage type even approaches this stress range.

In addition to the wide stress range of usage, the piezoresistance gages can be used over a wide range of time scales. By using thin gages, it is possible to achieve time resolutions of 20 ns in shock wave experiments. On the other hand, the same gages can be used for static loading situations. Even in field applications, measurements approaching static time scales have been obtained by suitable design of gage packages and allied instrumentation. Piezoresistance gages have also shown good survivability in fairly severe environments.[4] Because of the adaptability to a wide range of stresses, times, and their survivability in severe environments, we conclude that piezoresistance gages provide an impressive and unique measuring system.

In summary, the work to date has shown that piezoresistance gages are uniquely suited for experimental measurements, but that the interpretations of the data and error estimates are questionable because of the many complexities. These deficiences are recognized by workers in this area and the approach to date has been to minimize them by optimizing gage designs. For example, gage packages are designed and emplaced so that a particular component of stress (most often stress normal to the gage) has the largest contribution; strain compensation to correct for dimensional changes in divergent conditions have been attempted. These techniques, though useful and often necessary, cannot always be analyzed rigorously to provide quantitative estimates of error. Except for two papers,[17,30] discussed further in Section 3, theoretical work in this area has been lacking. To make optimal use of

piezoresistance gages, theoretical analysis and developments are
needed to supplement the experimental innovations.

1.3 APPROACH

To facilitate our discussion of the approach, we divide the investi-
gation on piezoresistance gages in to two parts: (1) the direct problem,
that is, determining the resistance change due to applied mechanical
loads, and (2) the inverse problem, that is, determining the state of
stress (or a specific component of stress) from resistance change measure-
ments. In this report we focus mainly on the direct problem. If we can
determine and model the resistance change due to applied loads and
separate out the contributions of the different phenomena discussed
in the last subsection, we can attempt to invert gage data in a particular
situation. Although inverting the gage data in a completely arbitrary
situation may never be possible, the work presented here should aid in
the design of gage packages to permit inversion of resistance change
measurements in specific situations.

To solve the direct problem, we first develop a continuum piezoresistance
model to relate the resistance change to mechanical loading. The past
data are reviewed and analyzed using this phenomenological model to
determine how and why the gages work and to identify the shortcomings in
previous studies. A few well-defined experiments are described to
examine the role of some key mechanical variables and to provide data
for analysis. A theoretical analysis is presented to examine the mechanical
interaction between the gage and the matrix. This analysis is checked
against experimental data to determine its validity and usefulness.

A brief discussion of the implications of this work for the inverse
problem is also presented.

Section 2

MODEL FOR PIEZORESISTANCE

This section describes a phenomenological model to calculate the resistance change in a gage element subjected to elastic-plastic deformation.[*] We can then examine how these relations may be inverted to provide stresses from resistance measurements. The development consists of incorporating plasticity in the piezoresistive relations presented by Mason and Thurston[33] for elastic solids. Some aspects of the work are similar to the developments presented in References 17 and 30; these papers are discussed further in Section 3.

Figure 2.1 shows an initial undeformed and a deformed configuration for the gage element. Our objective is to relate the resistance change between these two states--that is, to obtain expressions for resistivity changes and dimensional changes while simultaneously satisfying the mechanical constitutive relation. Throughout this work, we will assume material isotropy. The relations are in the incremental form and can therefore be used for large strains.

2.1 RESISTIVITY CHANGE DUE TO DEFORMATION

Mason and Thurston[33] presented the phenomenological development of piezoresistivity for elastic solids by considering the electric field E_m as a function of the current density J_m and stress σ_{ij}. This development is similar to other equilibrium and non-equilibrium processes that are based on a tensor formulation of the crystalline properties.[27] To extend this approach to elastic-plastic deformation, we proceed as follows.

The resistivity tensor and its components are defined using the generalized Ohm's law[+]

$$E_i = \rho_{im} \cdot J_m \tag{2.1}$$

---

[*] At present, we restrict our work to purely mechanical deformation and ignore thermal effects.

[+] Unless otherwise stated, we will use the summation convention and assume tensile stresses and strains as positive.

18
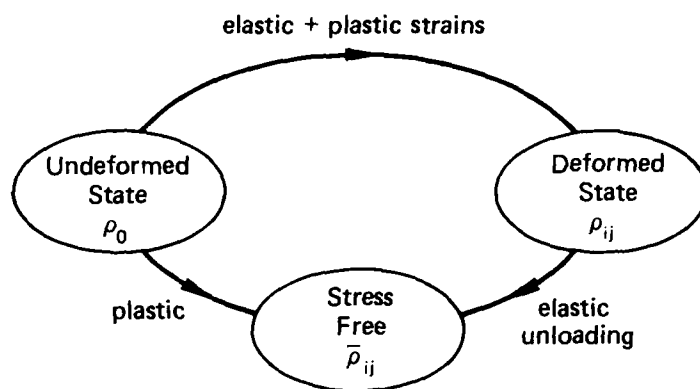
MA-8324-15

FIGURE 2.1   THE RESISTIVITY CHANGE $\Delta\rho_{ij}$ IN THE DEFORMED STATE

The stress-free state is a hypothetical state obtained by removing
all stresses (or elastic strains).

For cubic and isotropic materials, the resistivity ρ_{im} is a scalar:[27] $\rho_o \delta_{im}$, where δ_{im} is the Kronecker delta. The resistivity in the deformed configuration can be written as

$$\rho_{im} = \rho_o \delta_{im} + \Delta\rho_{im} \tag{2.2}$$

By considering the resistivity as a function of elastic strains (or stresses) and plastic strains, we can write

$$\Delta\rho_{im} = \rho_o \left[\left(\frac{\partial \rho_{im}}{\partial \sigma_{k\ell}} \right) \Delta\sigma_{k\ell} + \left(\frac{\partial \rho_{im}}{\partial \epsilon^p_{jk}} \right) \Delta\epsilon^p_{jk} \right] \tag{2.3}$$

$$= \Delta\rho^e_{im} + \Delta\rho^p_{im}$$

In the above expression, the partial derivatives imply that the other variable is being held constant. The first term represents the change in resistivity due to stresses (elastic strains) and is reversible if the stresses are removed. The second term represents an irreversible change in resistivity that is caused by production of lattice defects in the solid. For example, the second term is responsible for changes in the resistivity between an annealed and cold-worked material.

For discussing hysteresis later in this work, it is useful to define a stress-free state corresponding to the deformed configuration (Figure 2.1). The resistivity in this state can be expressed as

$$\bar{\rho}_{im} = \rho_o \cdot \delta_{im} + (\Delta\rho^p_o)\delta_{im} \tag{2.4}$$

Note that the stress-free resistivity is taken to be a scalar in agreement with our assumption of material isotropy.

In all of our work the term piezoresistivity applies only to the elastic term $\Delta\rho^e_{im}$.* This elastic component of the resistivity change

---

*Because plastic strains are also present, there is confusion in the shock wave literature. In the papers by Smith,[9] and Mason and Thurston,[33] only elastic solids were considered and the difference between strains and stresses was inconsequential.

is expressed as

$$\Delta \rho^{e}_{ij} = \rho_{o} \pi_{ijk\ell} \cdot \Delta \sigma_{k\ell} \qquad (2.5)$$

where the coefficients $\pi_{ijk\ell}$ are the appropriate partial derivatives from Eq. (2.3) and are components of a fourth-rank tensor termed the piezoresistive tensor. This tensor is similar to the compliance (or stiffness) tensor in elasticity as far as the nonzero and independent terms are concerned. There is, however, one major difference: Whereas elastic constants tend to be independent of the lattice defect density, the same is not true for the piezoresistive coefficients. Piezoresistive coefficients depend on heat treatment (e.g., annealed and cold-rolled foils have different coefficients).

Equation (2.5) is the fundamental relation underlying the use of piezoresistance gages for stress measurements. For cubic material, there are three independent components: π_{11}, π_{12}, and π_{44}. Here we have used the matrix notation and Equation (2.5), in this notation, is written as

$$\Delta \rho^{e}_{m} = \rho_{o} \pi_{mn} \cdot \sigma_{n} \qquad (2.5a)$$

where the subscripts range from 1 to 6 and the complete piezoresistive matrix is written as

$$\pi_{mn} = \begin{pmatrix} \pi_{11} & \pi_{12} & \pi_{12} & 0 & 0 & 0 \\ & \pi_{11} & \pi_{12} & 0 & 0 & 0 \\ & & \pi_{11} & 0 & 0 & 0 \\ & & & \pi_{44} & 0 & 0 \\ & & & & \pi_{44} & 0 \\ & & & & & \pi_{44} \end{pmatrix} \qquad (2.6)$$

For the present work, the interest is in isotropic materials and there are only two independent components π_{11}, π_{12} because $\pi_{44} = \dfrac{\pi_{11} - \pi_{12}}{2}$.

For isotropic materials, it is convenient to write Eq. (2.5) similar to Hooke's law

$$\Delta \rho^e_{ij} = \rho_0 \left[\alpha \Delta \sigma_{mm} \cdot \delta_{ij} + 2\beta \Delta \sigma_{ij} \right] \tag{2.7}$$

The constants α and β are material constants[*] similar to Lame's constants in elasticity. These constants can be obtained by measuring resistivity changes due to applied stresses in the elastic range.

The plastic component of the resistivity change is written similar to Equation (2.5)

$$\Delta \rho^P_{im} = \rho_0 \, \eta \Delta W^P \, \delta_{im} \tag{2.8}$$

where W^P is a scalar measure of plastic deformation and η is a material constant relating changes in plastic deformation (at constant stress) to resistivity changes. Two possible scalar measures of plastic deformation that may be used are

$$\Delta W^P = \sigma_{ij} \Delta \varepsilon^P_{ij}$$

or

$$I^P_2 = 1/2 \, (\varepsilon^P_{ij} \cdot \varepsilon^P_{ij})$$

The first measure is the plastic work and the second is the second invariant of the deviatoric plastic strain. At present, we do not know of any data for piezoresistance gages that can be used to evaluate Equation (2.8).

Combining Equations (2.7) (2.8), and (2.2), we can write the resistivity in the deformed state as

$$\rho_{ij} = \rho_0 \delta_{ij} + \rho_0 \left[\alpha \Delta \sigma_{mm} \delta_{ij} + 2\beta \Delta \sigma_{ij} + \eta \Delta W^P \delta_{ij} \right] \tag{2.9}$$

Equation (2.9) can be used to determine the resistivity change for a given mechanical loading, if the constants α, β, and η are known. We also point out that the stresses appearing in Eq. (2.9), for a given deformation,

_____

[*] $\alpha = \pi_{12}, \quad \beta = \left(\pi_{11} - \pi_{12} \right) \Big/ 2$

must be compatible with the mechanical constitutive model discussed in the next section.

The relations presented above are valid for large strains because they are in an incremental form. By making α and β a function of stress, we can include nonlinear terms. This procedure, though reasonable, is an approximation to a nonlinear theory. In the nonlinear theory, higher order terms in the Taylor's series expansion (Eq. 2.3) would need to be included. Given the present state of the art, we feel that our approach is adequate.

2.2 MECHANICAL CONSTITUTIVE MODEL

The resistivity changes due to deformation must be calculated in conjunction with the mechanical constitutive model. For purely elastic deformations of the gage, the plastic work term in Equation (2.9) goes to zero and stresses are readily known from Hooke's law. However, for an elastic-plastic response, the terms in the square brackets cannot be as easily determined from a knowledge of strains and an inelastic constitutive model must be considered.

Although several papers have reported the hydrostatic compressibility of piezoresistance materials, little data exist on the yield and deformation behavior for these materials. Also, when these data exist, they are of little value unless they are for the same material that was used in impact calibration studies. This is because the yield data, unlike compressibility data, are strongly dependent on impurities and heat treatment. Given the general lack of needed data, we will assume the simplest inelastic model: An elastic-perfectly plastic model. Work hardening can be easily added if future data warrant such an addition to the model.

The equations presented below are the usual textbook relations used for metal plasticity.[34] Stress is separated into deviatoric and spherical components

$$\sigma_{ij}' = \sigma_{ij} + \frac{\sigma_{mm}}{3} \delta_{ij}$$

23

Because these gages can be subjected to large compressive pressure P ($-\sigma_{mm}/3$), we express the pressure-volume relation as

$$P = A\mu + B\mu^2$$

where $\mu = D/D_o - 1$. D is the density and A and B are material constants.

Using the usual procedure for metals, we include all the inelasticity in the stress deviators. The equations in the incremental form are

(1) Additivity of elastic and plastic strain increments

$$\Delta\epsilon_{ij} = \Delta\epsilon^e_{ij} + \Delta\epsilon^p_{ij}$$

(2) Hooke's law for elastic strains

$$\Delta\sigma_{ij}' = 2G\Delta\epsilon_{ij}'$$

(3) Yield surface of the von-Mises type

$$f = \sqrt{J_2'} - Y = 0$$

where

$$J_2' = \frac{1}{2}\sigma_{ij}' \cdot \sigma_{ij}'$$

Work hardening can be included by making Y a function of plastic work W_p or plastic strain ϵ^p_{ij}. In accordance with the last subsection, Y also marks the onset of resistive hysteresis.

(4) Plastic Incompressibility

$$\Delta\epsilon^p_{mm} = 0.$$

Appendix A presents the elastic-plastic relations for some simple situations used in Section 3: One-dimensional strain ($\epsilon_y \neq 0$, $\epsilon_x = \epsilon_z = 0$) and a particular two dimensional strain ($\epsilon_x = \epsilon_y \neq 0$, $\epsilon_z = 0$). For arbitrary loading conditions, the imposed strain field in conjunction with our material model provides the stresses. These stresses in turn provide the resistivity change through Equation (2.9).

24

The elastic-plastic response of the gage is also responsible for the residual resistance (or gage hysteresis) observed in experiments. This hysteresis can have two contributions: (1) changes in the stress-free resistivity caused by the generation of lattice defects--that is, permanent resistivity changes, and (2) mechanical hysteresis--that is, residual stress and strains in the gage due to plastic deformation. Previous work[21] has attributed all of the hysteresis observed in shock wave experiments to changes in the stress-free resistivity. This is in error, particularly at low stresses, where the mechanical hysteresis contributions can be quite large. This topic is discussed further in Section 3.2.

2.3 USE IN EXPERIMENTS

In this subsection, we present the relations relating resistance changes to the imposed deformation. To aid writing the relations, we introduce the following nomenclature. We define a right-handed coordinate system (fixed on the gage element) such that the X axis is along the gage width, the Y axis is along the gage thickness, and the Z axis is along the gage length. All variables of interest will be transformed to this system.

In accordance with the experimental measurements, we will always consider the electric field $\vec{E}$ and the current density $\vec{J}$ along the gage length. The choice of coincident electric field and current vector eliminates any shear stress contribution to $\Delta \rho_{ij}$.[*] The resistance along the Z direction is written as[†]

$$R_Z = \frac{\rho_Z \cdot \ell_Z}{A_Z} \tag{2.10}$$

where $\rho_Z = \rho_{ZZ}$, ℓ_Z = gage length, and A_Z = area of cross section normal to the Z-direction. Denoting the variables in the initial state with the

---

[*] If the only resistivity changes of interest are $\Delta \rho_{11}$, $\Delta \rho_{22}$, $\Delta \rho_{33}$, then the form of the Π-matrix in Equation (2.6) does not permit contributions from $\rho_{ij} (i \neq j)$.

[†] No summation convention will be implied with capitalized subscripts.

subscript '0', we can write the resistance in the deformed state as

$$\frac{R_Z}{R_{Zo}} = \left(1 + \frac{\Delta\rho_Z}{\rho_Z}\right) \cdot \frac{\ell_Z}{\ell_{Zo}} \cdot \frac{A_{Zo}}{A_Z} \qquad (2.11)$$

Substituting for $\Delta\rho_Z$ from Equation (2.9) and defining the dimensional contributions by

$$\Delta\ell_i = \frac{\ell_i - \ell_{io}}{\ell_{io}}$$

We can write Equation (2.11) as

$$\frac{R_Z}{R_o} = \left[1 + \alpha\left(\Delta\sigma_X + \Delta\sigma_Y + \Delta\sigma_Z\right) + 2\beta\Delta\sigma_Z + \eta\Delta W^p\right] \frac{\left(1+\Delta\ell_Z\right)}{\left(1+\Delta\epsilon_Y\right)\left(1+\Delta\ell_X\right)} \qquad (2.12)$$

Equation (2.12) is the general relationship between the mechanical deformation and the resistance change measured by the gage. In the small strain approximation, the incremental quantities in Equation (2.12) can be replaced by their total values. In the remainder of this report, we have used this approximation.

Equation (2.12) shows the importance of knowing the strains in the gage element. A knowledge of these strains coupled with the constitutive model, permits the determination of stresses and hence the resistance change. We emphasize that the stresses and strains in Equation (2.12) are those in the gage element and not in the matrix. This point has not always been appreciated in past work[35] and is discussed further in Section 5.

In using piezoresistance gages, the objective is to invert the resistance measurement to determine a particular stress component in the matrix. From Equation (2.12) we can see that inverting the resistance change data is not a simple task. This then raises the question: How can the simple empirical relation given by Equation (1.1) be used when

26

the actual response (Eq. 2.12) is so complex? The resolution to this
question lies in the gage shape, gage plasticity, and the nature of the
shock wave uniaxial strain experiments. In Section 5, we show that for
a thin foil gage in a matrix subjected to uniaxial strain, the response
is determined primarily by the normal stress in the matrix. Thus, the
gage can be used to measure normal stresses provided the matrix is under
uniaxial strain. This simplification is not possible in general.

To invert Equation (2.12) for an arbitrary loading condition requires:
several gage measurements, knowledge of the various constants, and an
independent determination of the gage strains. Determination of α, β, η,
and the yield stress, although involved, can be made from well-defined
laboratory experiments. On the other hand, the determination of strains
is conceptually difficult because it depends on the specific situation
of interest (the gage-matrix interaction problem).

Independent measurements of strains have been considered in previous
work[26,35] to correct for dimensional changes in divergent flow conditions.
Using the developments presented in this section, we can examine the
requirements for using nonpiezoresistive materials to independently
monitor strains: (1) The material used for measuring strains should be
mechanically similar to the piezoresistance gage material and should be
placed similarly to the gages (see gage-matrix interaction in Section
5), (2) the coefficients α and β should be zero to ensure that stresses
or elastic strains do not result in resistivity changes, and (3) the
coefficient η, relating stress-free resistivity to plastic deformation,
in the two cases should be similar. These requirements are quite restric-
tive and point out the difficulty in accurately correcting for dimensional
changes.

27

SECTION 3

ANALYSIS OF PREVIOUS WORK

This section presents an analysis of past shock wave calibration data on Manganin and Ytterbium using the formulation given in Section 2. The thrust of the analysis is on reconciling shock wave data with hydrostatic measurements of resistance change to understand the response for different loading conditions. Previous analyses for these materials have been presented by Barsis et al.[17] (Manganin), and Grady and Ginsberg[30] (Yb). We have reanalyzed their data and extended the analysis to Lee's data[18] on Manganin. The procedure adopted here allows us to determine the adequacy in modeling the existing data, shortcomings in the analysis and/or data, and provides guidelines for improving the present understanding and usage of piezoresistance gages.

3.1 ANALYSIS OF MANGANIN DATA

Manganin has been extensively studied since 1964. Figure 3.1(a) shows the data from four studies.[16-18,35] These data are from Manganin foils and wires and the encapsulation materials range from epoxy to metals and hard ceramics. Except for Charest's data,[35] the data are in reasonably good agreement on this plot. Figure 3.1(b) shows only the data of Barsis et al.[17] and Lee[18] on a K versus normal stress plot.* Other data shown in Figure 3.1(a) have been left out because they are not as extensive and show a wide variation when compared with the data shown in Figure 3.1(b). Also shown is a horizontal line that represents the hydrostatic coefficient K(P) for Manganin. Both studies reported the same coefficient for hydrostatic loading. Barsis et al. used Manganin foil grids surrounded by epoxy and/or plasma-sprayed Al_2O_3 and these were shocked in a 2024 aluminum or 'ucalox matrix.[17] Lee used Manganin wire

---

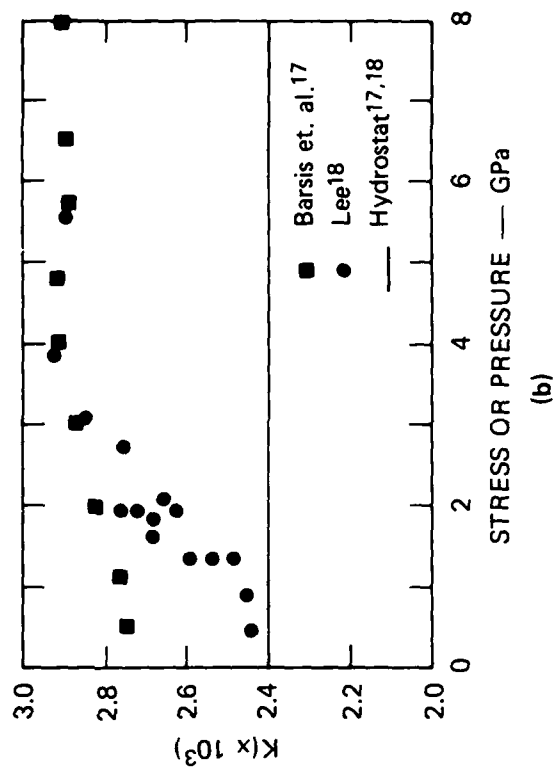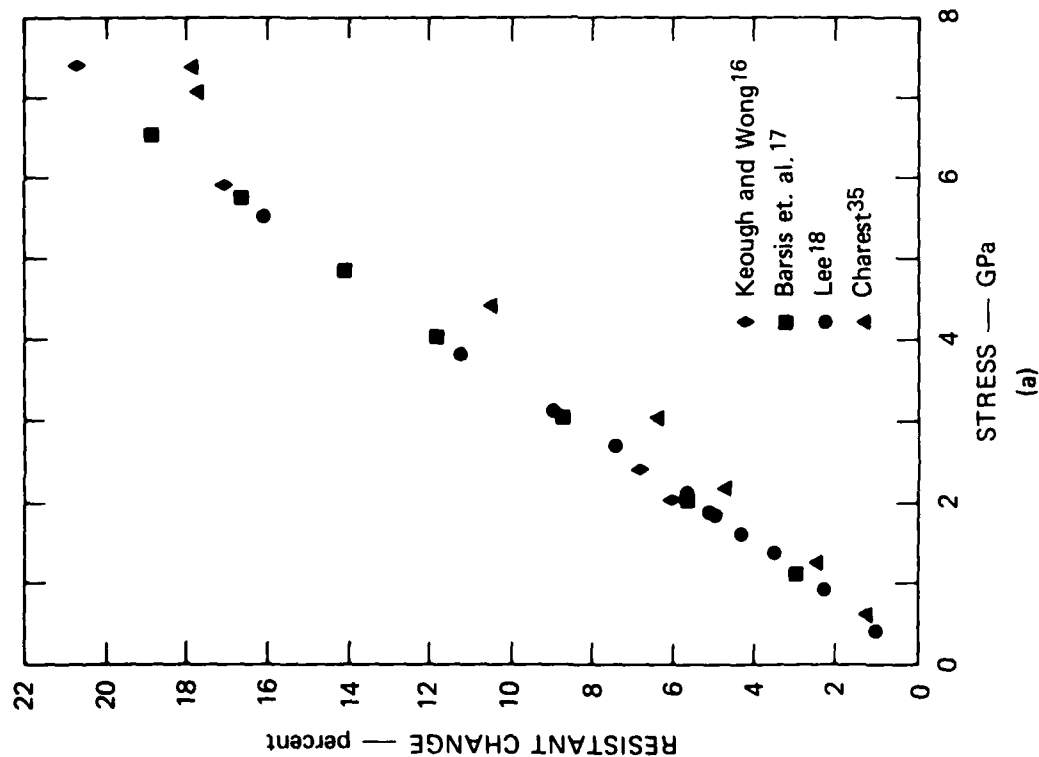* $K = \dfrac{\dot{R}}{R_0}/\sigma_n$; the K versus σ_n plot magnifies the scatter in data.

28

FIGURE 3.1 MANGANIN DATA FROM PREVIOUS STUDIES

(a) $\Delta R/R_o$ vs normal stress.
(b) K vs normal stress and hydrostatic pressure. The same coefficient for hydrostatic loading was reported by Barsis et. al. and Lee.

MA-8324-5

29

completely contained in C-7 epoxy. Above 30 kbar,[*] both sets of data are in good agreement and are approximately parallel to the hydrostatic line. Below 30 kbar the data have no clear patterns.

Barsis et al. appear to be the first investigators to consider a piezoresistivity tensor analysis for shock wave data. They also made the first quantitative attempt to explain the nonlinear $K - \sigma_n$ data shown in Figure 3.1(b) and to reconcile the shock wave data with hydrostatic measurements. The equation used by Barsis et al. to analyze their data is similar to Equation (2.12) with the following exceptions: (1) In their work they do not consider changes in stress-free resistivity; that is, the W^p term in Equation (2.12) is taken to be zero; (2) they choose to express their piezoresistive equations in terms of total strains; that is, instead of Equation (2.9), they use the following equation

$$ r_{ij} = r_o \cdot \delta_{ij} + 2r_\mu \epsilon_{ij} + r_\lambda \epsilon_{mm} \tag{3.1} $$

where r_{ij} is the resistivity. r_μ and r_λ are like α and β in our work. We believe that Equation (3.1) is incorrect because the resistivity changes are caused by stresses (or elastic strains) and not total strains. For example, if a conductor undergoes stress-free deformation, its resistivity cannot change.[+] As discussed below, we can simulate their analysis and results by setting β and η equal to zero in Equation (2.12). Also, $\epsilon_{mm} = \epsilon^e_{mm}$ in Equation (3.1) because of assumed plastic incompressibility.

A key aspect of the work by Barsis et al. was recognizing the importance of strain states in the gage and then attempting to account for them in the analysis. They analyzed their shock data assuming one- and two-dimensional strain states in the gage. They argued that the two-dimensional strain state ($\epsilon_x = \epsilon_y \neq 0$, $\epsilon_z = 0$) was a better representation

---

[*] We remind the reader that σ_n refers to the stress in matrix.

[+] Changes in stress-free resistivity due to the W^p term in Eq.(2.12) are not considered in the work by Barsis et al.

of the gage geometry* and differences in the Manganin and epoxy impedances. Their analysis was based on using $r_\mu = 0$ (similar to assuming $\beta = 0$ in our work). By assuming a two-dimensional strain state, they reconciled their shock and hydrostatic data and fitted the nonlinear response indicated by their data (Figure 3.1b).

We have analyzed the data of Barsis et al. and Lee's data using Equation (2.12). We emphasize that our procedure parallels the analysis by Barsis et al. because we assume $\beta = 0$ and $\eta = 0$. The analysis consisted of the following steps.

(1) The hydrostatic resistance data are converted to resistivity using the Manganin pressure-volume relation[17]

$$P = 1160\ \mu + 4120\ \mu^2 \qquad (3.2)$$

where $\mu = D/D_o - 1$ and P is in kbar. Appendix B shows how the dimensional term in Equation (2.12) can be expressed in terms of density changes.

(2) The resistivity-pressure data were used to obtain α (P)

$$\alpha = -\ 7.042 \times 10^{-4}\ (1 + 1.564 \times 10^{-4} P) \qquad (3.3)$$

(3) Using $\alpha(P)$, $\beta = 0$, $\eta = 0$, the resistance change can be computed from Equation (2.12) provided the stresses and strains are known. The normal stress in the gage is assumed to be the same as the matrix. By assuming a particular strain state, we can then calculate the other stresses (Appendix A). The yield stress (Y°) used in these calculations is 2 kbar.[17]

Figure 3.2 shows the calculated curves for one- and two-dimensional strains and the data from Figure 3.1(b). The agreement between the two-dimensional strain curve and the data of Barsis et al. merely confirms their result. However, the data of Lee agree better with the one-dimensional strain curve. This is difficult to explain because the wire geometry used by Lee more closely approximates two-dimensional strain than the geometry used by Barsis et al.

*Because of the large length (compared to width and thickness), there is no strain along the gage length. In the other two directions, the gage is compressed equally because Barsis et al. treat the epoxy like a fluid.

31
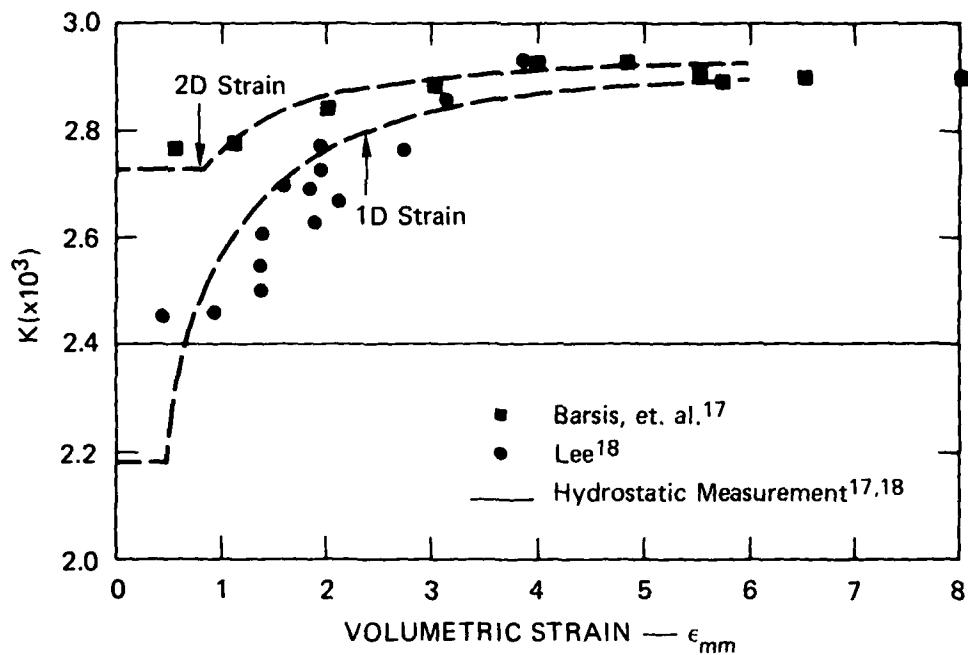
FIGURE 3.2   COMPARISON OF EXPERIMENTAL DATA ON MANGANIN
WITH ELASTIC-PLASTIC CALCULATIONS

The 1D and 2D strain states refer to the assumed state of strain
in the foil.

Figure 3-2 clearly shows the importance of gage plasticity on resistance change. However, at stress levels in excess of 50 kbar, the one- and two-dimensional strain differences become negligible and the behavior is similar to hydrostatic response except for an offset. The results presented in Figure 3.2 have an inherent error because resistance hysteresis was not taken into account either in the experimental data or in the analysis. The papers by Lee and Barsis et al. mention the observations of resistance hysteresis, but do not report any results. The results in Figure 3.2 are discussed further in Section 3.3.

3.2 ANALYSIS OF THE YTTERBIUM DATA

Ytterbium gages have been extensively studied under shock loading by Ginsberg et al.[21] Resistance change measurements under hydrostatic loading have been reported by Lilley and Stephens.[36] In the work by Ginsberg et al., the gages were encapsulated in epoxy-fiber glass sheets and the gage packages were then shocked in a variety of matrix materials. By conducting impact experiments at various velocities, these authors obtained the resistance change for different stress levels ranging between 50 MPa and 3 GPa. Their calibration data are shown in Figure 3.3(a). In addition, these authors have also presented the residual resistance (upon longitudinal unloading in the matrix) as a function of peak stress, as shown in Figure 3.3(b).

Grady and Ginsberg[30] have presented an analysis of their resistance-stress data using the relation

$$\frac{\Delta R_i}{R_o} = \pi_{im}\sigma_m + G_{in}\epsilon_n \qquad (3.4)$$

where the matrix notation (m and n range from 1 to 6) is used for stresses and strains. Because the current and the electric field vectors are coincident, i values ranging between only 1 and 3 need to be considered. π_{im} are the piezoresistive coefficients and G_{in} is a matrix used to write the dimensional terms in a compact notation.

33
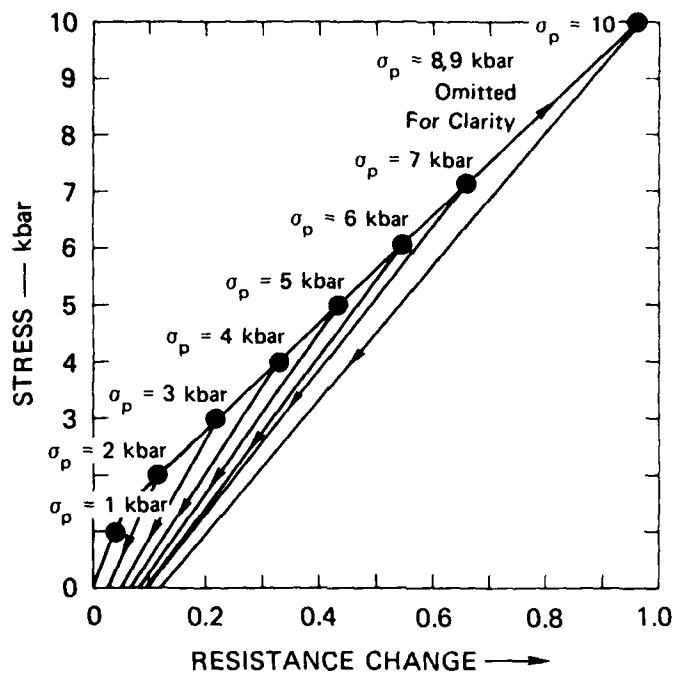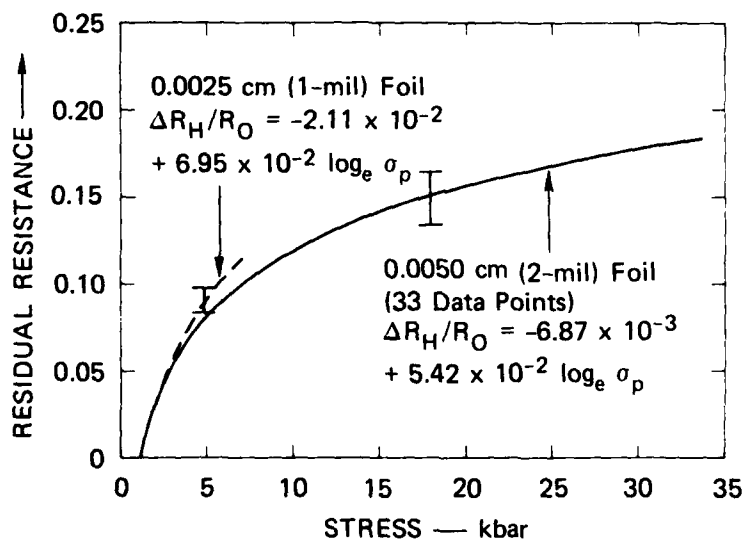
FIGURE 3.3   YTTERBIUM DATA FROM GINSBERG et. al. (Ref. 21)

(a) Resistance change as a function of peak stress.
(b) Residual resistance as a function of peak stress.

$$G = \begin{pmatrix} 1 & -1 & -1 \\ -1 & 1 & -1 \\ -1 & -1 & 1 \end{pmatrix}$$

Equation (3.4) is identical to $(R_z/R_{zo} - 1)$ obtained from Equation (2.12) if η is set equal to zero.

Assuming a one-dimensional state of strain* in the ytterbium, Ginsberg and Grady obtained the following results:

(1) Using Equation (3.4) they analyzed resistance change data in the elastic range under hydrostatic[36] and tensile loading to obtain π_{11} and π_{12}. These in turn were used to correctly predict the uniaxial strain data at low stresses (elastic region) and provided further confidence in the π-values.

(2) They extended their elastic resistance-stress calculation into the plastic region by arguing that beyond yielding, the deformation of Yb is hydrostatic. Thus, hydrostatic data for resistance change[36] can be directly used to extend their theoretical curve to higher stresses.

(3) They showed good agreement between their theoretical curve (step 2 above) and shock data by subtracting the measured residual resistance [Figure 3.3(b)] from the resistance change at peak stress [Figure 3.3(a)].

Grady and Ginsberg concluded that hydrostatic and shock wave data in Yb can be explained by assuming a one-dimensional strain state, using a piezoresistivity tensor analysis and subtracting the residual resistance. Unfortunately, steps 2 and 3 are in error. Step 2 is incorrect because the procedure used by the authors is valid for resistivity changes and not resistance changes. The dimensional term is different during hydrostatic and uniaxial strain compression, as discussed in Appendix B.

Step 3 is incorrect because not all of the residual resistance is caused by changes in the stress-free resistivity (referred to as plastic resistivity change in Section 2). Some residual resistance is expected

---

*These authors argued that the compressibility of the epoxy-fiber glass composite was similar to the ytterbium.

35

from purely mechanical hysteresis. The residual resistance shown in
Figure 3.3(b) is for zero longitudinal stress. The other stresses are
not zero and they contribute to the resistance change through Equation
(2.12). Appendix C explains how these values can be calculated. Here
we simply present the results: For a peak stress of 2 kbar, the residual
resistance due to nonzero stresses and strains contributes 75% to
the residual resistance; at 4 kbar peak stress this contribution drops
to 41%. With increasing stress, the contribution of purely mechanical
hysteresis to resistance change decreases and the change in stress-free
resistivity becomes more important. This is because the residual stresses
are limited by the magnitude of the yield stress.

We have reanalyzed the data of Ginsberg et al. using Equation (2.12)
in a manner similar to that used for the Manganin data in the last sub-
section. The following procedure was used

(1) The resistance change data under hydrostatic pressure[36] were
changed to the resistivity data using the following fit to the
pressure-volume data on Yb.[37]

$$P = 146.65 \, \mu + 122.05 \, \mu^2 \qquad (3.5)$$

where $\mu = D/D_o - 1$ and P is in kbar*

(2) The resistivity-pressure data were used to obtain α (P)

$$\alpha = -0.02 - 7.24 \times 10^{-4} P \qquad (3.6)$$

where we have assumed $\beta = 0$. For Yb, the choice of $\beta = 0$ is
supported by the values of π_{11} and π_{12} reported by Grady and
Ginsberg.[30] (Note, their analysis is valid in the elastic
range.) Whether this approximation is valid for higher
stresses is not known.

(3) Using $\alpha(P)$, $\beta = 0$, and $\eta = 0$ in Equation (2.12), we can
calculate the resistance change provided the stresses and
strains are known.†

---

*P is positive in compression.

†The use of $\eta = 0$ in determining the theoretical value is reasonable
since we are going to approximately correct for this in the experimental
data.

Figure 3.4 shows the calculated points of K versus σ_n by assuming one and two-dimensional strains in the ytterbium. The pressure-volume relation used is given by Equation (3.5), and Y^o (the yield in simple tension) was taken to be 0.6 kbar. The yield limits for one-and two-dimensional strain states, corresponding to Y^o, can be calculated from Appendix A. Figure 3.4 also shows the peak resistance change, peak minus the total residual change (procedure used in Ref. 30), and the peak minus the residual change consistent with assumptions of one-dimensional strain and an elastic-perfectly plastic solid.* The difference in these latter two curves is due to the contribution of mechanical hysteresis; the relative magnitude of this contribution decreases with increasing stress. At low stresses, the one-dimensional strain calculation gives a better fit to the data; at higher stresses, the two-dimensional strain calculation gives a better fit to the data. At very high stresses, the state of strain becomes less important.

3.3 Discussion

The analyses presented show that the theoretical model outlined in Section 2 is necessary for understanding the shock response of piezoresistance gages and for attempting to reconcile these data with data from other loading conditions. The importance of gage plasticity in explaining the nonlinearities in the experimental data is quite evident from the comparisons between theory and experiment. The analysis of the ytterbium data shows the difficulty in correctly accounting for the resistance hysteresis.

A key aspect of the comparison between theory and experiment is a knowledge of the stresses and strains in the gage itself. The differences in the results for the assumed one-and two-dimensional strains are clearly seen for low and moderate stresses. Because these differences are directly related to gage plasticity, they are less important at very high stresses. The choice of one-dimensional and two-dimensional strains in the analysis

---

*
Rigorously, even this procedure is incorrect because the subtracted amount represents the plastic contribution upon longitudinal unloading and not at the peak.
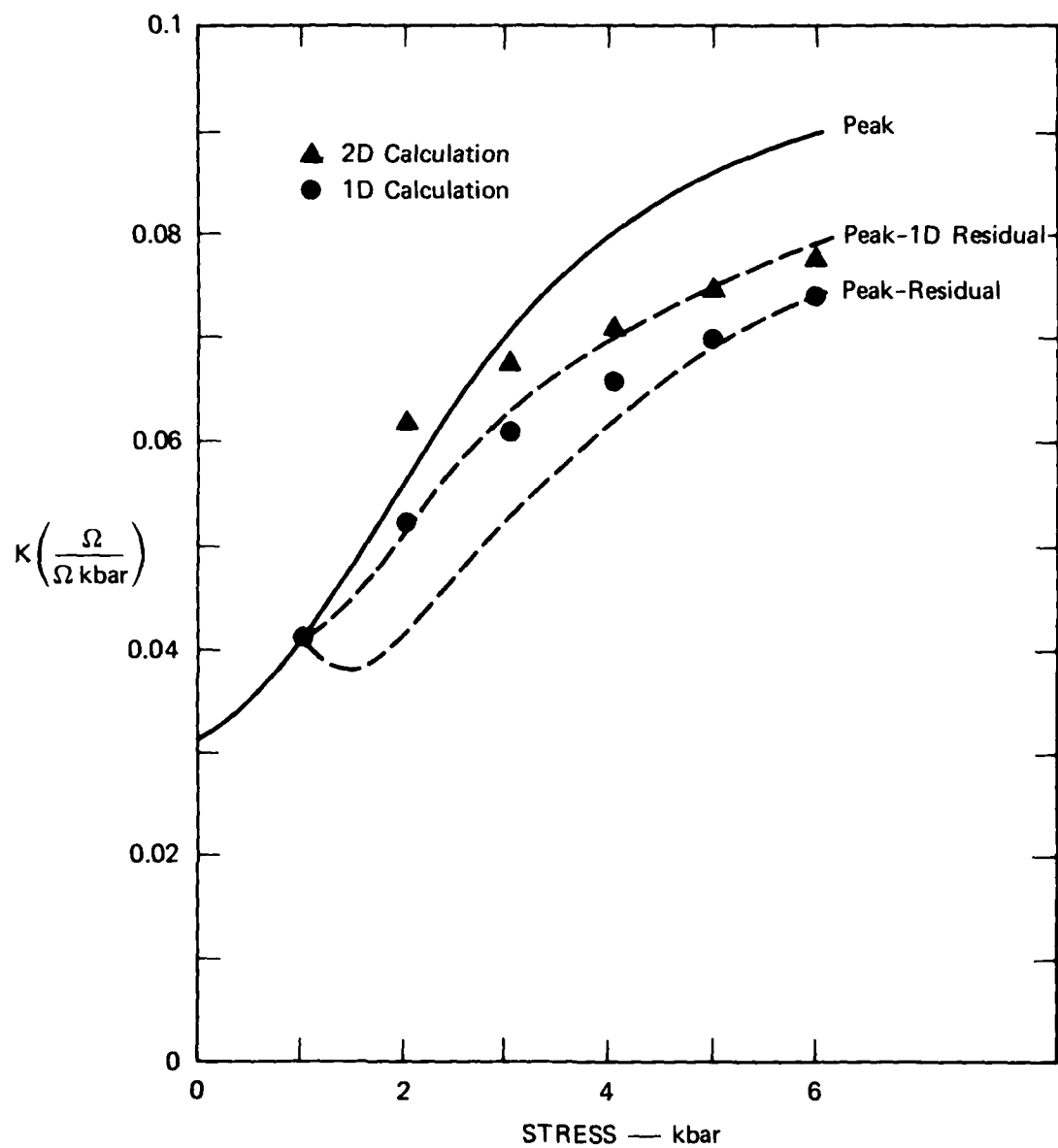
FIGURE 3.4 COMPARISON OF EXPERIMENTAL DATA ON YTTERBIUM WITH ELASTIC-
PLASTIC CALCULATIONS.

MA-8324-8

38

is governed, in part, by the fact that these states are easy to analyze.
The exact state of strain in the gage is difficult to determine. Further-
more, in all of the analyses it was assumed that the normal stress
in the matrix was identical to the normal stress in the gage. Although
this assumption appears reasonable (if the gage is envisioned as a
thin planar sheet), it has not been rigorously demonstrated. We
speculate that violation of this assumption may explain, in part, the
differences between Lee's data[18] and the results of Barsis et al.[17]
The cylindrical cross section of the wire gage used in Lee's work is
expected to be a larger perturbation to the matrix stresses than the
foil gage. Earlier work by Keough and Wong on Manganin wires and
foils showed that wire response in contrast to foil response was more
influenced by the matrix response.[15] Section 5 discusses the question
of gage-matrix interaction in more detail.

The analyses presented provide insight into how these gages
work and how they can be used in an empirical manner for uniaxial
strain in the matrix. If the normal stress in the gage and the matrix
is the same, then the gage plasticity restricts the magnitude of the
other stresses for a given strain state. The onset of the plastic
response and the relationship between the various stresses is determined
by the strain state. The strain state, in turn, depends on the form of
the foil grid and the material surrounding it.

The continuity of normal stress can be assured by using a thin
foil* (see Section 5 for rigorous proof), and the strain states can be
kept approximately identical in all cases by choosing a particular
grid pattern and surrounding it by a similar epoxy resin in each case.
Such a gage (or gage package) can then be calibrated and used in an
empirical manner (Eq. 1.1) for shock wave uniaxial strain experiments.
Irrespective of the matrix material, the gage response will then be
governed by only one quantity--normal stress in the matrix. The litera-
ture, shows that the gages are generally used in this manner. Because
of differences in gage material and gage fabrication, different

---

*The use of wire gages should be minimized or eliminated.

39

investigators have provided calibration data for their particular gage. Selection of one grid pattern and a well-characterized gage material would be highly desirable because it would eliminate the need for repeated calibration studies.

We have not discussed gage hysteresis because it is expected to be reproducible, since the gage response is governed by the matrix normal stress. For using the gage only in uniaxial strain experiments, the empirical procedure used by Vantine et al.,[32] to account for hysteresis may be satisfactory.

The above remarks apply only to the use of piezoresistance foil gages in shock wave uniaxial strain experiments. If these gages are to be used in more general loading situations, then their behavior needs to be examined for those particular situations. The response to more general loading conditions cannot be directly extrapolated from shock wave uniaxial strain data. This issue is considered in Sections 5 and 6.

Section 4

EXPERIMENTS ON PIEZORESISTANCE FOIL GAGES

The experiments were designed to determine the effect of well-
defined changes in mechanical loading on the gage response. The objectives
of the experiments were to: (1) determine the effect of stress rotation
in the matrix on gage response, (2) compare stress-resistance data in a
truly uniaxial strain geometry with conventionally used foil geometry,
and (3) determine sensitivity to shear deformation. These experiments
provide self-consistent comparisons and are not intended to provide
calibration data.

Ytterbium was chosen as the piezoresistance material because it
exhibits a large change in resistance at low stresses, thereby increasing
the measurement accuracy. There also exist considerable piezoresistance
and mechanical data for comparison with our experimental and analytic
results.[*] Partially offsetting these positive aspects, however, is the
batch-to-batch variability in material texture and resistivity. As noted
earlier, Yb foils are not as reproducible as Manganin foils. We felt we
could eliminate this problem by comparing results from gages constructed
from uniform regions of one foil. We were not entirely successful, as
indicated by the results in this section.

In the impact experiments, the piezoresistance gage response is
related to the stress state in the surrounding matrix. Hence, it is
important that the matrix material be well characterized for loading
conditions of interest. Furthermore, the matrix material should permit
a good bond with the gage; that is, the measurements should not be perturbed
by intermediate layers of dissimilar material. To satisfy these requirements.
we chose Polymethyl Methacrylate (PMMA) as the matrix material. The work
by Barker and Hollenbach has provided extensive, accurate uniaxial strain

---

[*] We have used Yb foils from the same supplier, and with similar material
preparation, as that used in the work of Ginsberg et al.[21]

41

data on PMMA.[38] More recently, the compression and shear wave studies by Gupta[39] have provided a complete determination of the stress-tensor in PMMA under uniaxial strain loading. The knowledge of the complete stress tensor is needed for an analysis of the results, particularly for the experiments in Section 4.1.

In all of our experiments, the gages were embedded in the PMMA. The general technique consisted of grooving the size of the gages and bonding the gage by a thin layer of epoxy (Hysol 815, which closely matches PMMA). The PMMA surface containing the gage was lapped to ensure that the specimen and the gage surface were flush. PMMA blocks were bonded to these surfaces using very thin Hysol bonds. Specific configurations for each experimental type are described in the following subsections. The experiments in 4.1 and 4.2 were conducted with the SRI 10-cm-diameter gas-gun.[40] The shear loading experiments in 4.3 were conducted with the 6.35-cm-diameter inclined impact facility.[41]

4.1 ROTATION OF MATRIX STRESSES

Figure 4.1(a) shows the gage emplacement for stress measurements. Gages denoted by '1' have the configuration that is normally used in shock wave experiments. For these gages the direction of shock propagation is normal to the major surface of the foil. Gages denoted as '2' are identical to the '1' gages, but are rotated 90° with respect to the shock propagation direction. Thus, to an observer, in the gage coordinate system, the matrix stresses for the two sets of gages appear to have been rotated. By comparing the output from the two sets of gages, we can determine the effect of stress rotation on the gage response.

An important aspect of this experiment involves the feasibility of measuring lateral stresses in shock wave experiments.* If the gage

---

*An important limitation in existing shock wave uniaxial strain data is the inability to determine the lateral stresses. This limitation is caused by the absence of experimental methods to measure lateral stresses and by the absence of lateral stress terms in the conservation equations describing uniaxial strain flow.[42] Shock wave results are completely described by the longitudinal stress-volume-energy (σ_x-v-E) relation.

Shock Direction
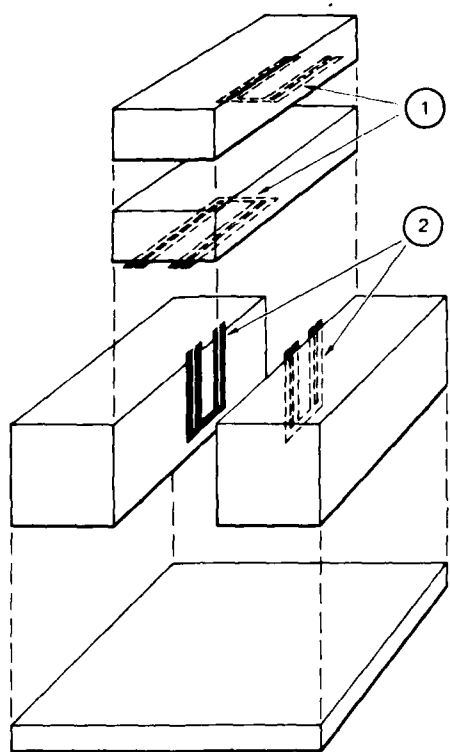
MA-8324-11

(a)
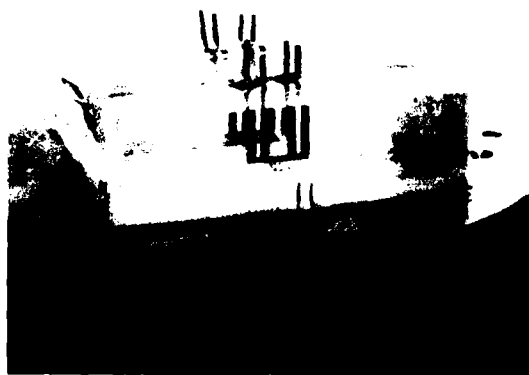
MA-8324-12

(b)

FIGURE 4.1   EXPERIMENTAL ASSEMBLY FOR STRESS MEASUREMENTS

(a) Schematic view of unassembled blocks showing the four gages.
(b) Assembled target.

responds only to the stress component normal to its major surface, then gages denoted as '2' should measure the lateral stress in the matrix. We point out that the idea of using piezoresistance gages to measure stresses other than the longitudinal stress is not new; the first attempts, using Manganin wire gages, were those of Bernstein et al.[43] It is not possible to analyze each experiment here in detail, but some general observations and difficulties with the past work[43-45] are summarized below.

The use of wire gages is not appropriate because a wire element appears identical to the stress wave for both longitudinal and lateral stresses unless it is contained in a planar slab of another material. In the contained situation, the in-situ nature of the measurements is compromised and two-dimensional wave effects need to be examined. Two of the previous studies[43,45] used Manganin, which gives appreciable signals, only at high stresses. At high stresses, the matrix material is difficult to characterize because of dynamic yield and failure. This difficulty, coupled with the complex nature of the gage package, does not permit a clear interpretation of the results. Stubbs et al.[44] examined the use of carbon gages to measure lateral stresses at low compressive stresses (∿10 kbar). They corrected many of the problems related to encapsulation techniques for lateral stress measurements and qualitatively demonstrated the potential for measuring lateral stresses. Quantitative evaluation of their work is difficult because of a lack of independent stress determination in the matrix material, the uncertainties in carbon gage calibration, and the difficulty in understanding the true response of the gage because of the many layers of encapsulation of materials in the gage package. The lack of an independent stress determination in the matrix is particularly important because without such a determination it is difficult to establish the validity of using a piezoresistance stress gage for lateral stress measurements. Previous studies have not always appreciated this point and have reported lateral stress measurements without appropriate demonstration of gage calibration. In summary, given the complex nature of piezoresistance measurements and the complexities indicated above, previous studies have not unambiguously demonstrated the use of piezoresistance gages for quantitative measurements of lateral stresses.

In our experiments we have avoided the above-cited difficulties by embedding gages directly in PMMA. Specifically, the experimental procedure was as follows. PMMA blocks, shown in Figure 1(a), were accurately machined to give flat and parallel surfaces (tolerances ≈0.0025 cm). The blocks were grooved to the dimensions (length = 25.4 mm, width = 2 mm, depth = 0.05 mm) required for emplacing Yb gages. The gages were set in the grooves using Eastman 910 adhesive at a few points and the very small clearance around the gages was filled with a material that matches the mechanical impedance of PMMA. After the gages were set in the PMMA blocks, the faces with the gages were carefully lapped to ensure that all gages were flush with the PMMA surface. The blocks were then bonded together using the filler material. An assembled target with the 4 four-terminal gages is shown in Figure 4.1(b). The use of a rectangular foil without encapsulating layers is in contrast to previous studies using encapsulated grids.

Two experimental assemblies were constructed with two gages of each type in each experiment. In the first experiment, the filler material was PMMA powder dissolved in ethylene dichloride solution.[46] The ethylene dichloride was also used for bonding the blocks. In the second experiment, the filler and bonding material was Hysol 2038 epoxy resin. The change of the bonding material in the second experiment merely reflects experimental convenience and is not expected to influence the conclusions drawn from this work.

Projectile velocities were chosen to give a compressive stress amplitude of 0.5 GPa in these experiments. At this stress level we have independently established the magnitude of lateral (or deviator) stresses for uniaxial strain in the PMMA matrix. Resistance change methods were made using the usual four-probe measurements. In addition, impact tilt and projectile velocities were monitored. The resistance changes from the two experiments are shown in Figures 4.2(a) and 4.2(b) respectively and the results, summarized in Table 1, are discussed next.

(a)

MA-8324-13

(b)
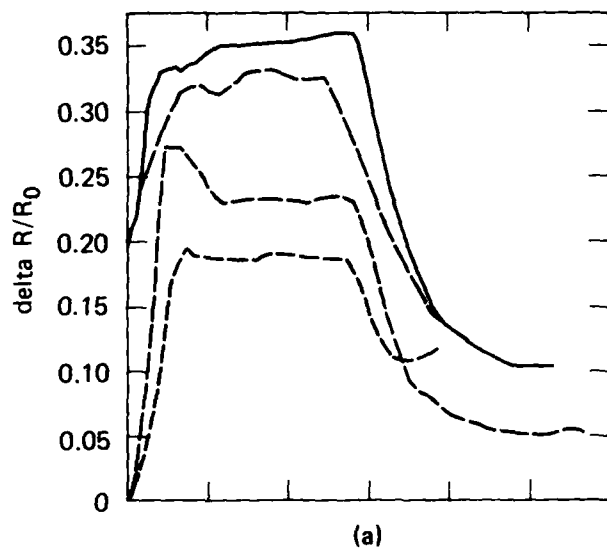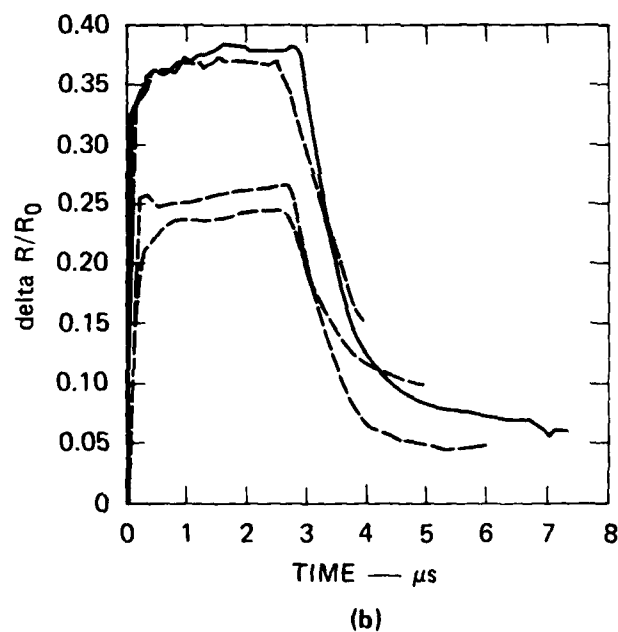
MA-8324-14

FIGURE 4.2   RESISTANCE CHANGE DATA FROM THE TWO EXPERIMENTS

The data have been normalized to wave arrival times.
The higher amplitudes are from the gages measuring longitudinal stresses,
while the lower amplitudes are from the gages measuring lateral stresses.

46

Table 4.1

EXPERIMENTAL RESULTS OF MATRIX STRESS ROTATION EXPERIMENTS

Experiment	Proj. vel. (mm/μs)	Long. stress[*] σ_x (kbar)	Lat. stress[*] σ_y (kbar)	Ratio[*] σ_y/σ_x	Measured resistance change[†]		Measured resistance change ratio
					$(\Delta R/R_o)_1$[‡]	$(\Delta R/R_o)_2$[§]	
1	0.28	5.1	2.83	0.57	0.34 ± 0.02	0.21 ± 0.02	0.62 ± 0.09
2	0.29	5.3	3.05	0.58	0.38 ± 0.01	0.245 ± 0.015	0.64 ± 0.06

[*]These values are determined from a knowledge of PMMA Hugoniot and the corresponding dynamic mean stress-volume relation determined in Reference 39.

[†]The error bars reflect the scatter between the two gages.

[‡]For this gage, the direction of shock propagation is normal to the gage plane.

[§]For this gage, the direction of shock propagation is parallel to the gage plane.

47

The resistance change data from the first experiment (Figure 4.2a)
showed considerable scatter. However, the differences between the two
sets of gages are quite marked. To reduce this scatter, we obtained the
four gages for the second experiment from a small area of one foil. The
results of the second experiment (Figure 4.2b) indeed showed less scatter
and confirmed the results of the first experiment. Table 4.1 gives the
ratio of lateral and longitudinal stresses in the matrix and the measured
resistance change ratio from the two sets of gages. Within experimental
scatter these values agree,[*] suggesting that resistance changes are governed
by the stress component normal to the major surface of the foil. More
work needs to be done to improve experimental precision and to extend the
results to other stress amplitudes.

Although the resistance change ratio measured here agrees with the
expected stress ratio, it is difficult to reconcile this result with the
calibration data for Yb shown in Figure 3.3. Those data show a nonlinear
resistance change above 0.1 GPa. From the measured resistance change
ratios shown in Table 4.1, we obtain stress ratios ranging between
0.71-0.73 using the calibration data of Ginsberg et al.[†] These values
are higher by about 20% in comparison with the calculated values. The
point to be made here is that the calibration data for one orientation
cannot be directly used for gage measurements along a different orientation;
separate calibration data are required for each orientation. Extending
this result, we can see the potential for even a larger error when gage
data from one loading condition are used for a different loading condition.

In conclusion, the results of the matrix stress rotation experiments
show that the resistance change ratio for the two orientation is in
reasonable agreement with the ratio of stresses normal to the major foil
surfaces. However, separate calibration curves are needed for the

---

[*] The average measured values are higher than the calculated values.

[†] Because our gage configuration and construction is different from that
of Ginsberg et al., the use of their data cannot be justified for an
absolute calibration. However, their data are suitable for comparisons.

two orientations. More experiments of the type presented here are required to provide confirmation of present results at other stress levels and to examine the development of a stress gage for measuring lateral stresses in uniaxial strain experiments.

4.2 EFFECT OF STRAIN STATE ON FOIL RESPONSE

The precise form of the strain state in a foil has generally not been considered in shock calibration experiments. However, a uniaxial strain state is often assumed[21] because: (1) the width-to-thickness ratio of the foil is large, and (2) the compressibility difference between the foil (particularly Yb) and the surrounding epoxy is small. To determine the validity of the one-dimensional strain approximation and to measure the true one-dimensional strain response, we conducted shock experiments on piezoresistance foils of several different widths. Because the lateral boundaries influence the final strain state in the foil, a sufficiently wide foil will initially be in uniaxial strain compression, whereas a narrow foil will rapidly be in biaxial strain compression. We can determine the effect of foil strain state by comparing the time-resolved piezoresistance response of both foils to a rapidly rising stress pulse in the matrix material.

The experimental configuration of these experiments is shown in Figure 4.3. Three foils, each of 0.005 cm thickness, were cut in four terminal arrays, as shown, from one large piece of foil. The widths of the gages were 0.05, 0.32, and 2.54 cm, respectively. Each was bonded with Hysol 815 epoxy in milled grooves and the specimen assembly was completed as described previously to ensure good lateral (edge) contact to the PMMA.

Resistance measurements were made by pulsing each foil with constant currents of equal current density (A/cm^2) in each foil and observing the time-resolved voltage developed across a section of the foil. Currents of ~100 A were used in the 2.5-cm foil to obtain adequate signals. Stress amplitudes of ~0.2 GPa and 0.5 GPa in the PMMA matrix were chosen to optimize the experimental conditions.

49
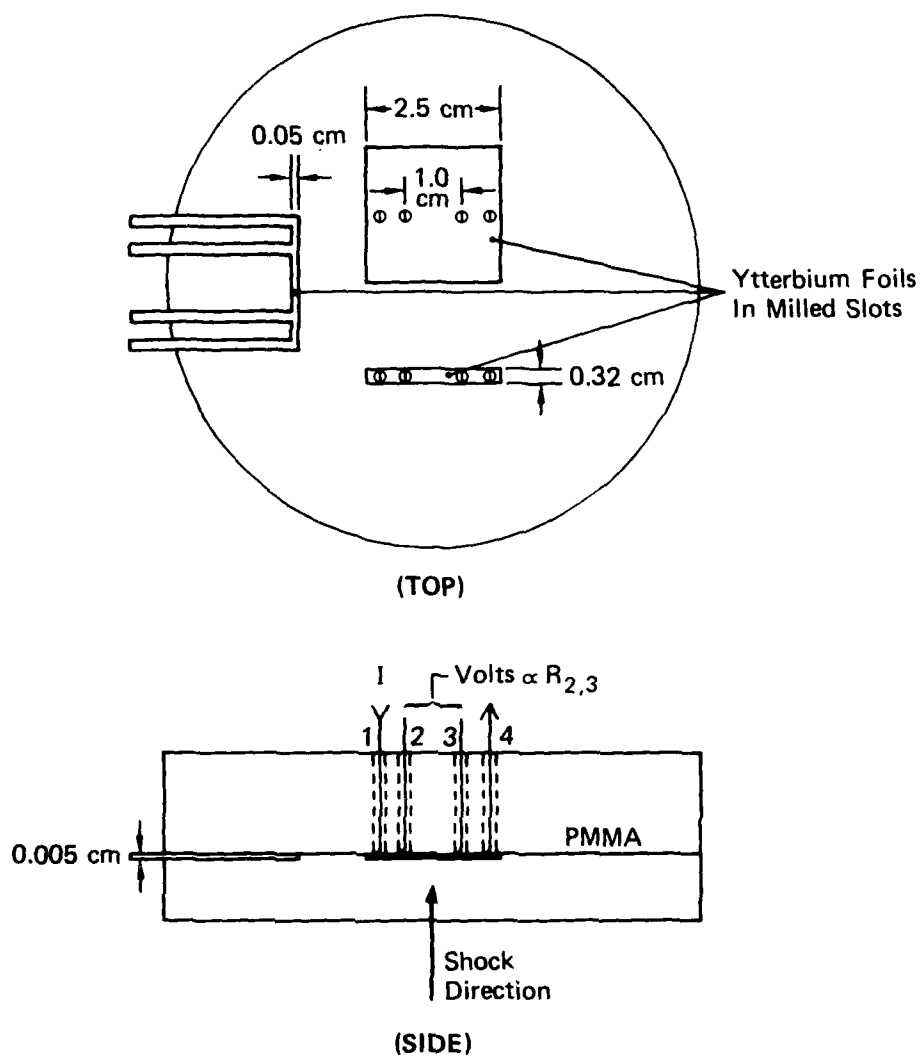
FIGURE 4.3   UNIAXIAL AND BIAXIAL STRAIN CONFIGURATIONS

Contacts to Ytterbium foils are 0.005 cm thick copper foils
soldered to vapor deposited copper tabs on Ytterbium.

Initial and average resistance changes obtained in three experiments are shown in Table 4.2. It can be seen that the ordering of response is not consistent; that is, changes in resistance do not correlate with width. In two of the experiments (0.2 and 0.55 GPa), the narrow foils responded essentially the same. In the other (0.48 GPa experiment), they differed substantially (~24%). With the exception of the one value for the 2.54-cm foil at 0.55 GPa, all points are considerably lower than the data of Ginsberg et. al.[21]

The time response results are shown in Figures 4.4, 4.5, and 4.6. Here again the results are inconsistent. At the lower stress level, 0.2 GPa, considerable noise obscures the data; however, the average values of the narrow foils are essentially the same. (Data for the 2.54-cm foil were not obtained because of equipment malfunction.) In the 0.48-GPa experiment, all foils exhibited no change with time (within the precision of measurement, ~2%). However, in the 0.55-GPa experiment (Fig. 4.6), the widest foil showed a decrease of ~12% with time.

A comparison of our shock compression data with those of Ginsberg et al.[21] is shown in Figure 4.7. Our data indicate considerably lower values of resistance change for a given stress in the matrix than those in Reference 21. We have not been able to account for this difference.

We conclude from these experiments that:

(1) The values measured for the narrowest foils in our work are consistently lower than those for similar foils in previous work.[21] These differences are beyond the experimental scatter and may be due to differences in strain states and/or differences in foil material.

(2) We cannot detect an influence of boundaries for Ytterbium in PMMA. It should be noted that these materials do not differ substantially in compressibility. A larger difference might be obtained with a greater mismatch.

Table 4.2

RESISTANCE CHANGES IN UNIAXIAL STRAIN EXPERIMENTS

Experiment Number	Stress (GPa)	Foil Width (cm)	$\Delta R/R_0$		
			Initial	Average*	Residual
1	0.20	0.05	-	0.09	-
		0.32	-	0.09	-
2	0.48	0.05	-	0.35	-
		0.32	-	0.26 ± 0.01	-
		2.54	-	0.31 ± 0.01	-
3	0.55	0.05	0.38 ± 0.02	0.37 ± 0.12	0.09 ± 0.01
		0.32	0.38 ± 0.002	0.36 ± 0.02	0.08 ± 0.02
		2.54	0.565 ± 0.03	0.49 ± 0.04	0.16 -

*Average of resistance changes at a given stress.
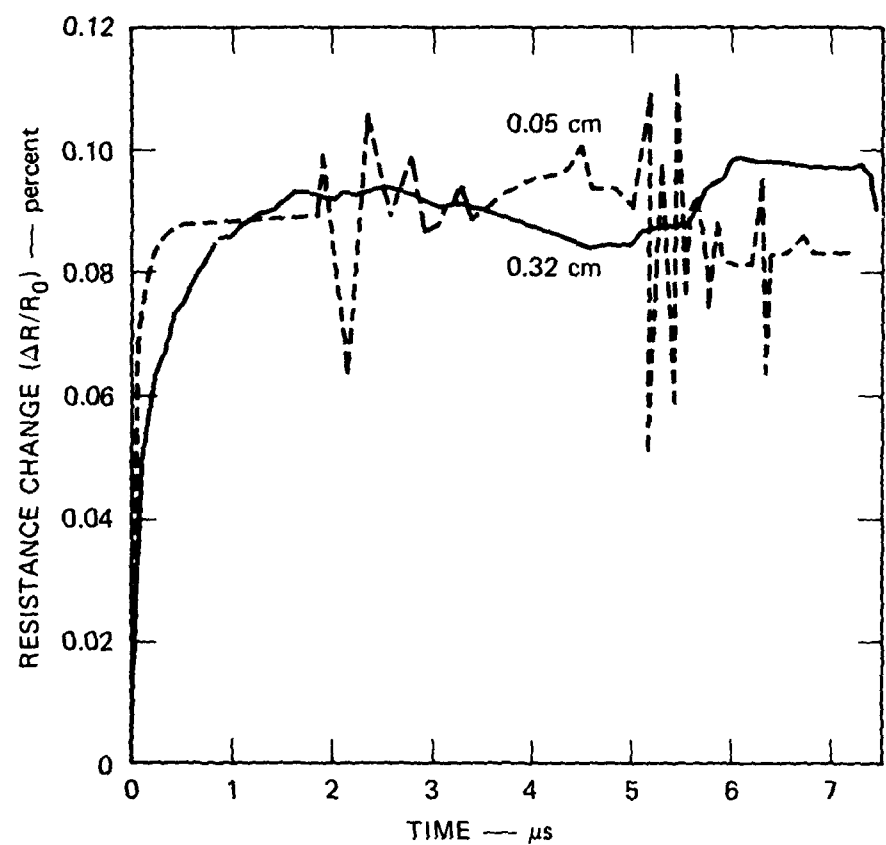
MA-8324-4A

FIGURE 4.4   RESISTANCE CHANGE VERSUS TIME FOR YTTERBIUM
FOILS (Stress of 0.2 GPa in PMMA)

The foil widths are indicated in the figure.
Other dimensions were the same.

53
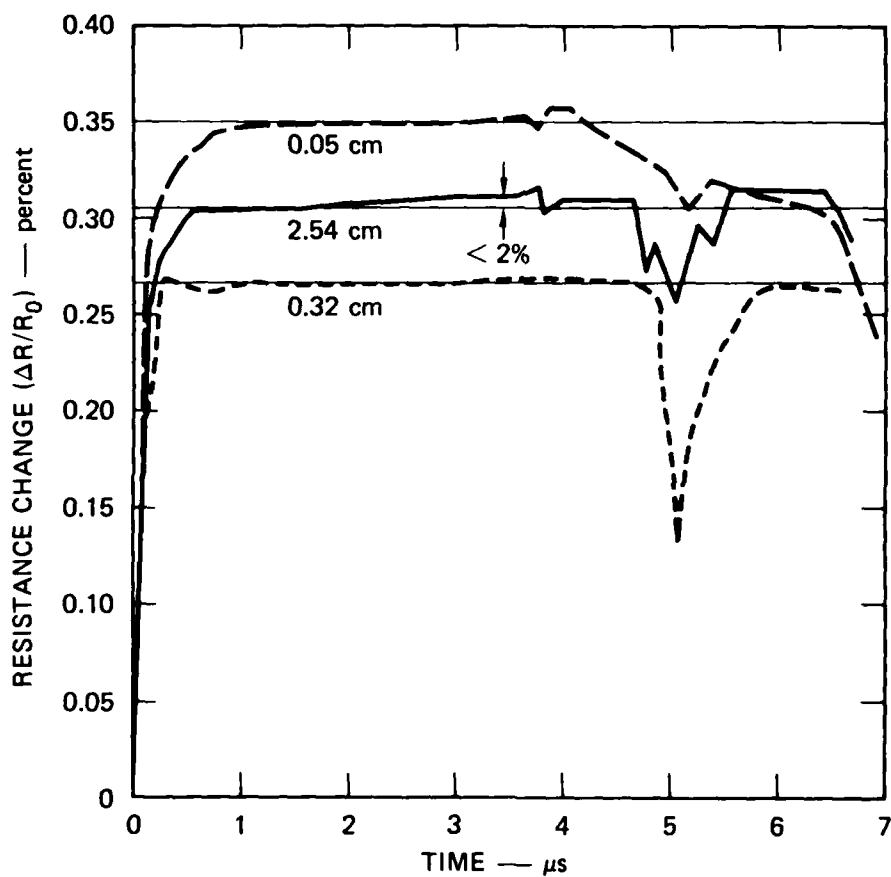
FIGURE 4.5   RESISTANCE CHANGES VERSUS TIME FOR YTTERBIUM
FOILS (Stress of 0.48 GPa in PMMA)

The foil widths are indicated in the figure.
Other dimensions were the same.

RESISTANCE CHANGE ($\Delta R/R_0$) — percent
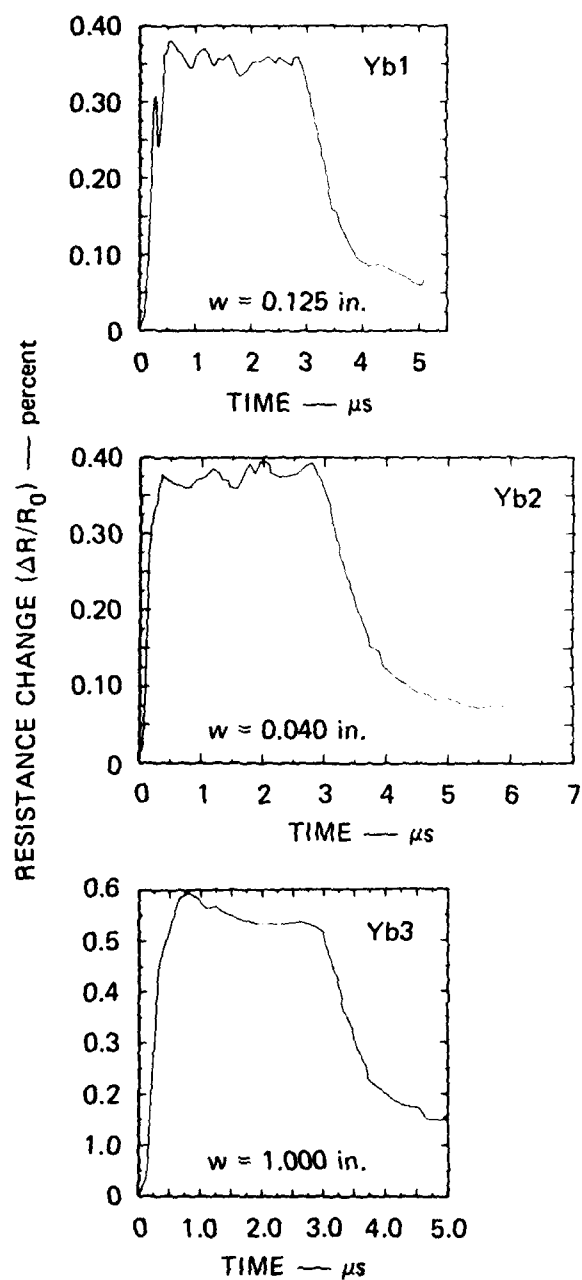
MA-8324-16

FIGURE 4.6   RESISTANCE CHANGES VERSUS TIME FOR YTTERBIUM
FOILS (Stress of 0.55 GPa in PMMA)

The foil widths are indicated in the figure.
Other dimensions were the same.
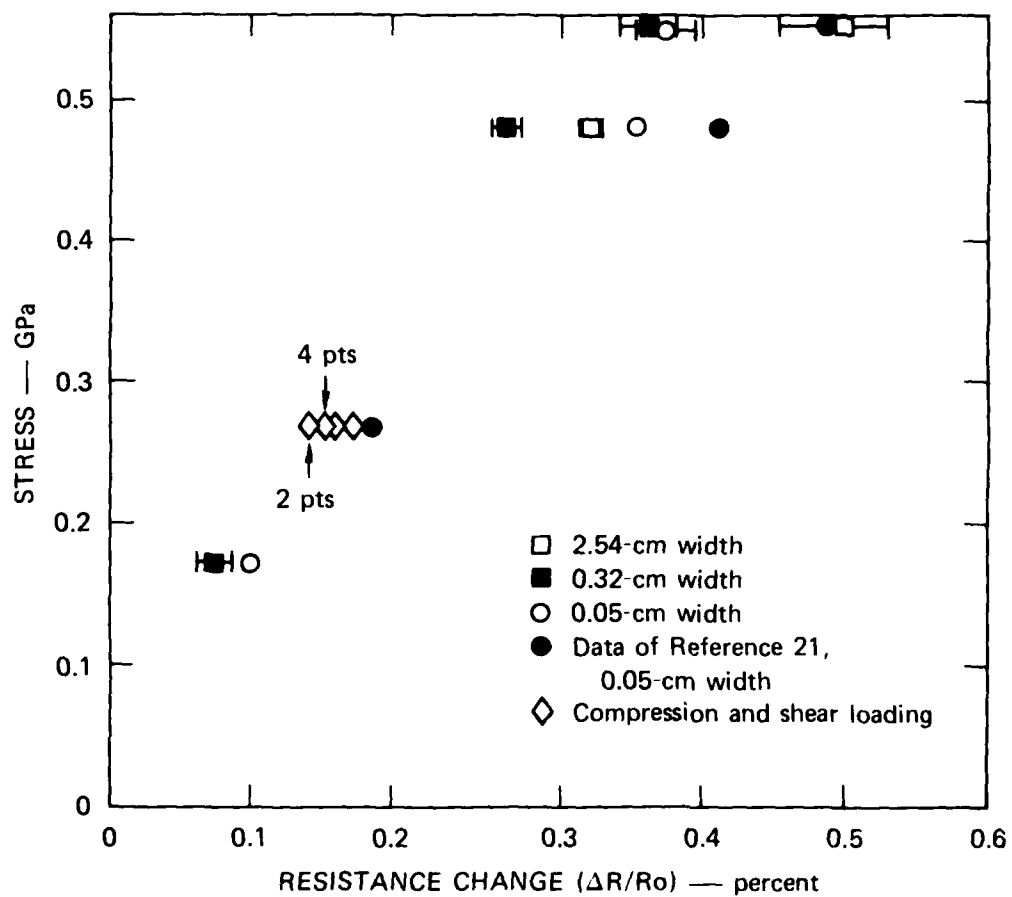
MA-8324-17

FIGURE 4.7   MATRIX (PMMA) NORMAL STRESS VERSUS Yb. RESISTANCE CHANGE

4.3 EFFECTS OF SHEAR LOADING

In field tests, shear deformations may be induced in piezoresistance gages. These deformations can result from non-normal incidence of stress waves or from shear waves in the test medium. An examination of the piezoresistive theory presented in Section 2.1 shows that shear stresses should not induce a change in the resistivity. This result is due to the form of the piezoresistive matrix and because of coincident current and electric field vectors (see discussion in Section 2.3). However, the presence of shear stresses in the foil can alter the compressive stresses due to plasticity and can, therefore, change the resistance measurements.

To examine the above effect due to shear deformation, we conducted combined compression and shear experiments on ytterbium foils embedded in PMMA. The gage emplacement is similar to that described earlier in this section. Gage foils were aligned so that the applied shear stresses were along the gage length and the gage width, as shown in Figure 4.8.

The technique for producing combined compression and shear loading is described in the paper by Gupta et al.[47] and is shown in Figure 4.9. Parallel, inclined plates are impacted to produce compression and shear waves in the specimen. Because of wave separation in the specimen interior (due to wave velocity differences), the response of the piezoresistance gages can be obtained for each wave.

The response of the PMMA under combined compression and shear loading, using particle velocity gages, has been determined independently by Gupta.[39] We have, however, conducted one experiment using particle velocity gages to determine the shear stress across the interface and the precise wave arrival times for the experimental configuration of interest to the present work. This experiment was similar to the piezoresistance target assembly shown in Figure 4.8, except that a particle-velocity gage was substituted for the piezoresistance gages.
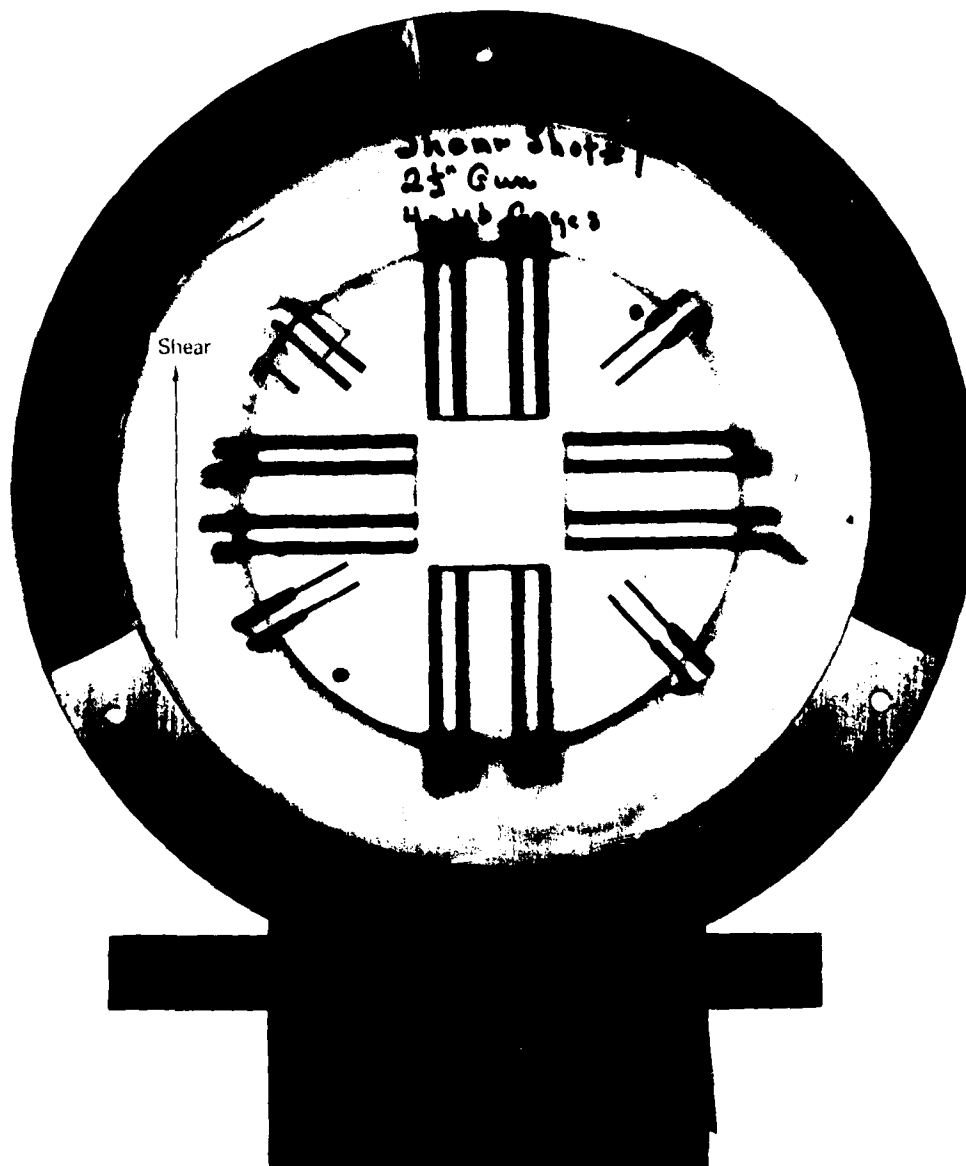
MP-8324-18

FIGURE 4.8   FOIL CONFIGURATION IN SHEAR LOADING EXPERIMENTS
(View from impact side).

For gages 2 and 3, the direction of shear is along the length;
for gages 1 and 4, the direction of shear is along the width.
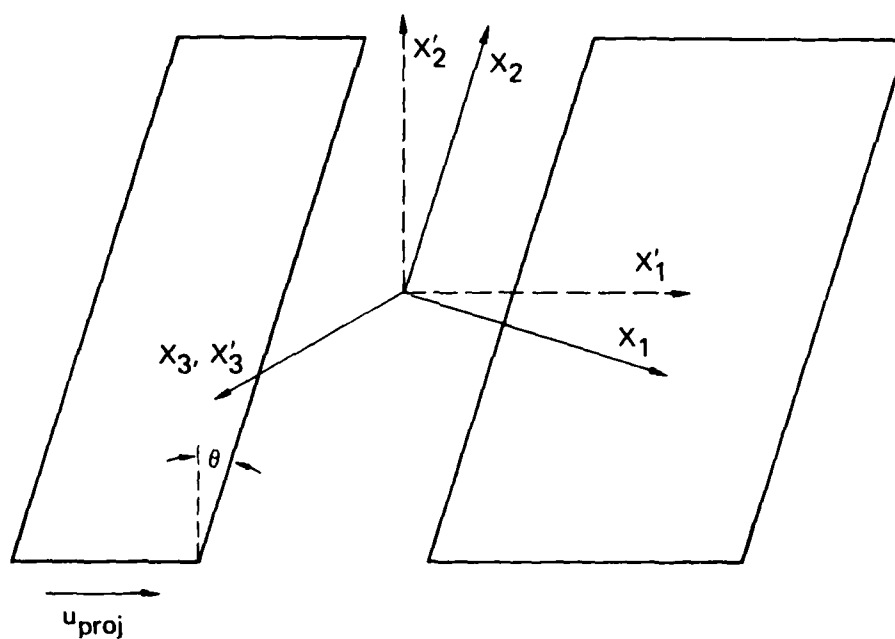
FIGURE 4.9 SCHEMATIC VIEW OF EXPERIMENTAL TECHNIQUE TO PRODUCE COMPRESSION AND SHEAR WAVES

The X'_i refers to the laboratory system; X_i refers to the coordinate system fixed on the impact plates.

The data from this particle-velocity gage experiment are shown in Figure 4.10. These consist of a voltage-time profile at the impact surface (PV1) and in the specimen interior (PV2) at a plane equivalent to the Yb foil gage experiments (~0.51 cm from the impact surface). The experimental setup was designed to provide signals only from the shear wave. However, the errors in the magnetic field alignment and finite impact tilt cause a small signal from the compression wave (the small precursor in the PV2 profile). Because there is no separation of waves at the impact surface, the impact surface gage (PV1) shows no such precursor. An analysis of these data gives the following results

Wave separation = 1.47 μs

Compression stress = 2.7 kbar[*]

Shear stress = 0.34 kbar.[*]

These results show that a considerable shear stress is transmitted through the specimen interior.

Results from the piezoresistance gage experiments are shown in Figure 4.11 and 4.12. As can be seen, there is a considerable amount of scatter for a constant stress input. The results in Figure 4.11, however, show a discernable change upon shear wave arrival. The results in Figure 4.12 are not as clear. Average resistance values for intervals corresponding to the compression wave only (<1.47 ms) and to combined compression and shear (1.47 to 3.1 μs) are shown in Table 4.3. The average increase in the resistance change is ~10% in the first experiment and ~2% in the second. The first value is larger than the experimental uncertainty, whereas the second value is well within experimental uncertainty.

The results of our experiments indicate an effect of shear stress on the gage response. Unfortunately, because of the lack of reproducibility in the data, the conclusions cannot be considered definitive.

---

[*]The compression stress was calculated using the jump conditions and by writing the particle velocity as one-half the longitudinal component of the projectile velocity. The shear stress was also obtained by using the jump conditions. The measured shear wave and particle velocities were used.
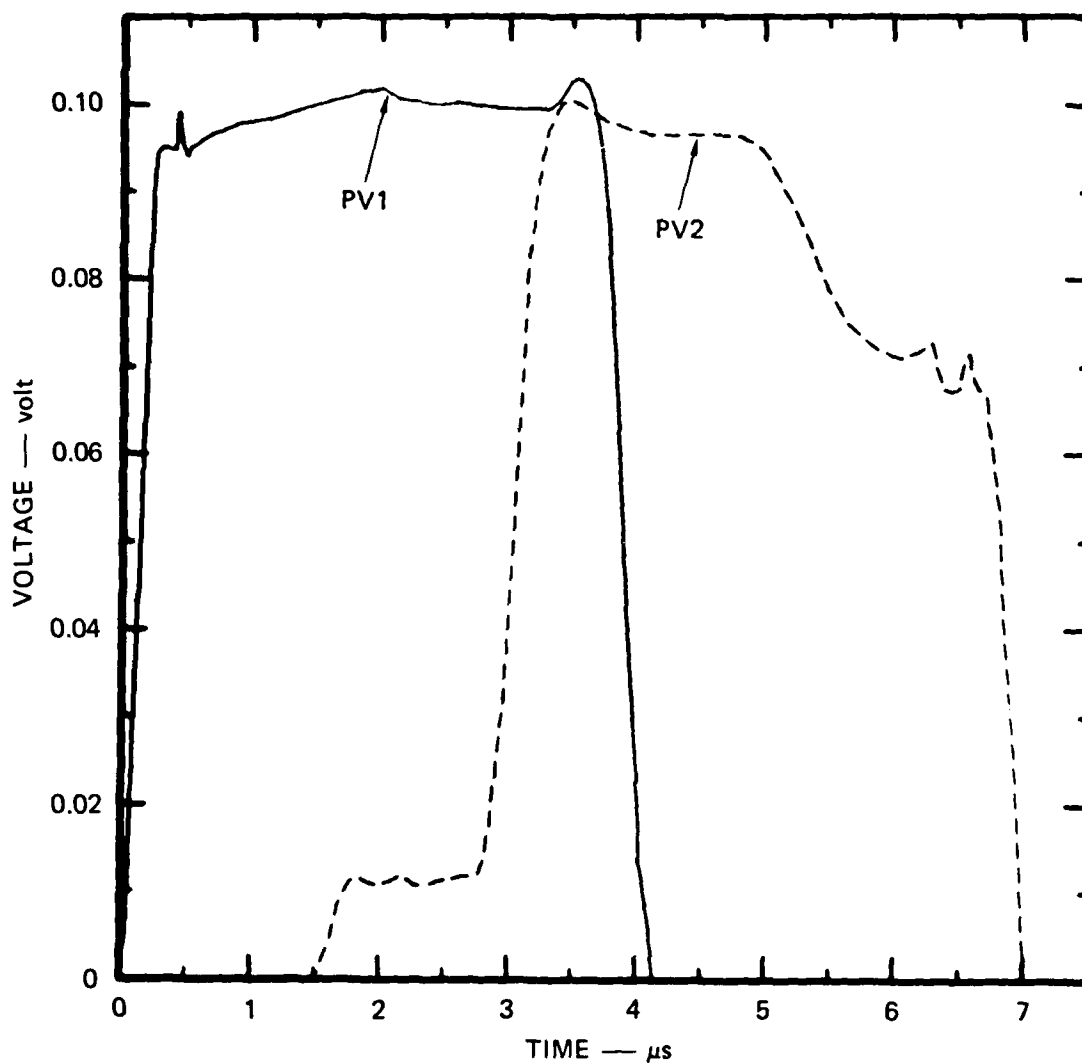
MA-8342-19

FIGURE 4.10 PARTICLE-VELOCITY DATA (voltage versus time profile) FOR AN IMPACT
SURFACE AND INTERIOR GAGE UNDER COMBINED COMPRESSION
AND SHEAR LOADING

The small precursor in the PV2 signal is caused by the longitudinal wave.
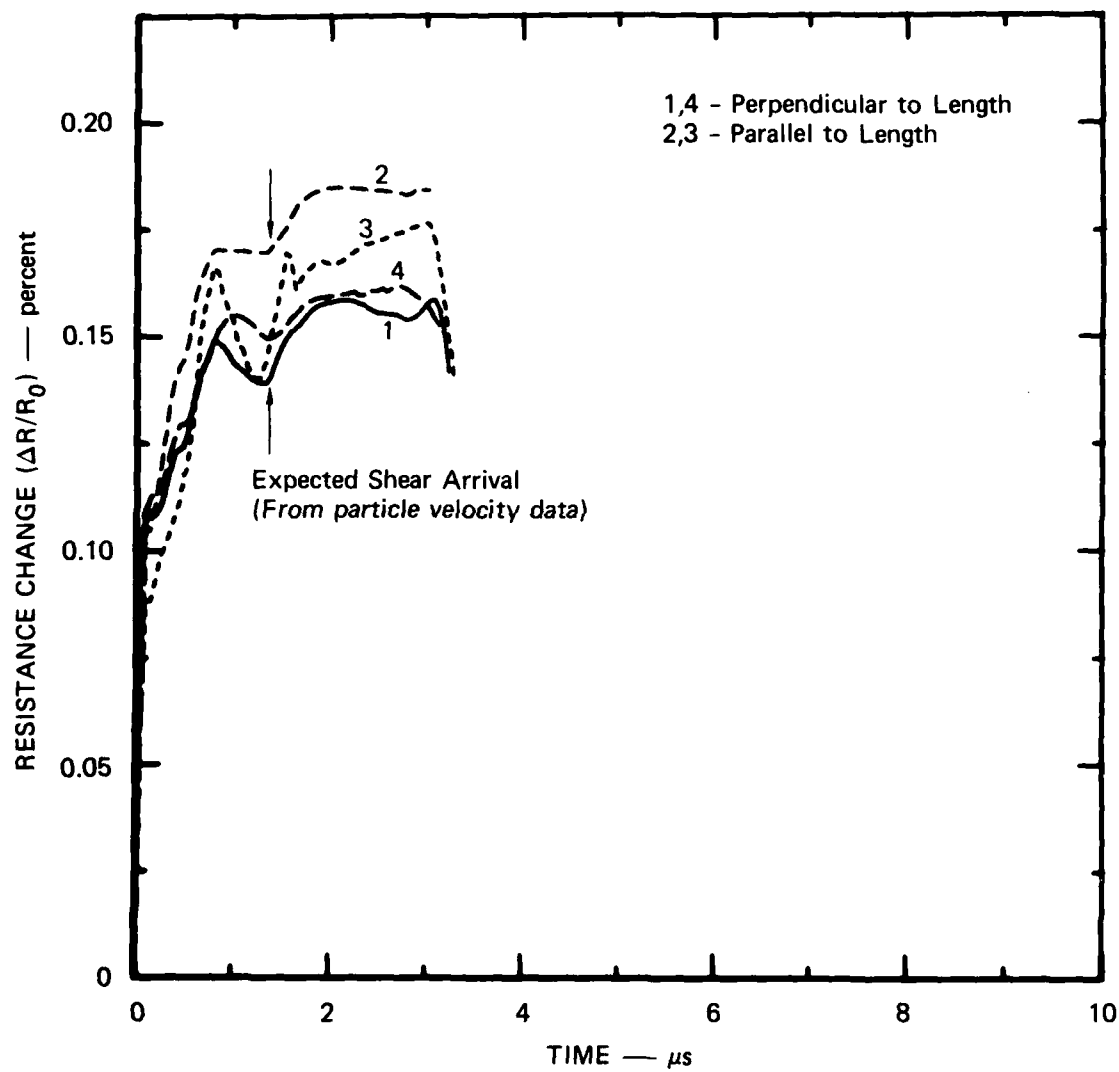
FIGURE 4.11 RESPONSE OF Yb GAGES TO COMBINED COMPRESSION AND SHEAR LOADING

62
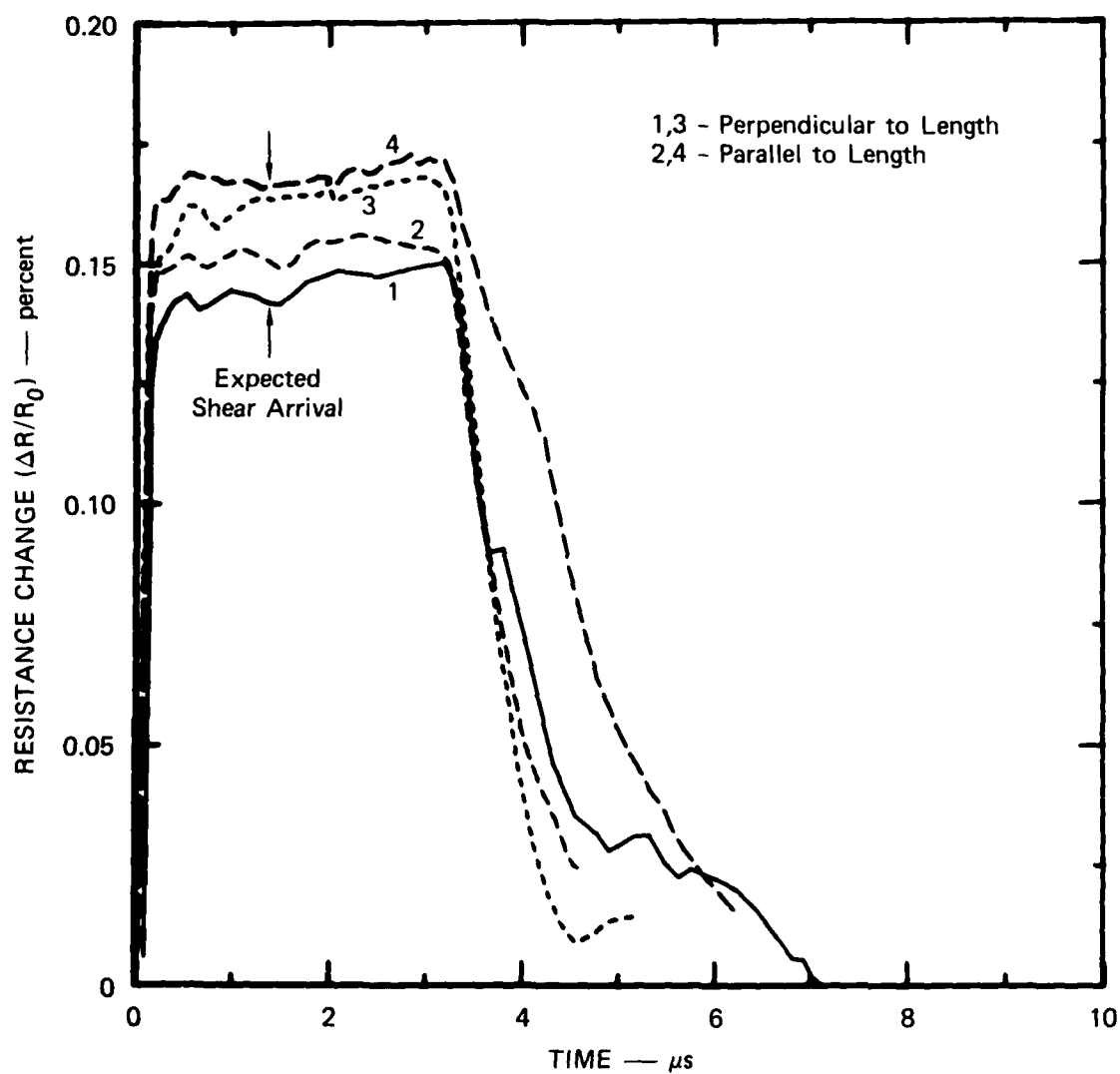
FIGURE 4.12 RESPONSE OF Yb GAGES TO COMBINED COMPRESSION AND SHEAR LOADING

Table 4.3

DATA FROM COMPRESSION AND SHEAR LOADING EXPERIMENTS

Gage No.	Stress (GPa)		$\overline{\Delta R}/R_o$		$\dfrac{(\Delta R/R_o)_s}{(\Delta R/R_o)_c}$
	Compression	Shear	$0.5 < t < 1.47$ μs	$1.47 < t < 3.2$ μs	
1*	0.27	0.034	0.154	0.167	1.08
2†			0.164	0.175	1.07
3†			0.152	0.167	1.10
4*			0.149	0.168	1.13
1*	0.27	0.034	0.152	0.153	1.0
2†			0.151	0.153	1.01
3*			0.163	0.168	1.03
4†			0.168	0.172	1.02

* Shear along width of gage.
† Shear along length of gage.

64

4.4 SUMMARY

The experiments described show that the mechanical variables considered
in this work influence the gage response. Unfortunately, the lack of
reproducibility in the results described in Sections 4.2 and 4.3 does
not permit firm conclusions regarding the effect of strain states and
shear deformation. More work is needed to clarify these effects.

The experimental results from matrix stress rotation show that the
gage responds primarily to the stress normal to its major surface.
Furthermore, the calibration for gages in one orientation is not
applicable to the other orientation. This raises the question: How can
we explain or model the response of the gages in the two orientations?
In the last section we assumed continuity of normal stress and a
particular strain state to derive the resistance change of gages
oriented in the usual orientation (designed to measure longitudinal
stresses). Similar assumptions cannot be used for the other orientation
(designed to measure lateral stress), because it is difficult to determine
the stresses and strains in the foil. The answer to the above question is
obtained by modeling the gage as an inclusion in the matrix, as described
in Section 5.

SECTION 5

DETERMINATION OF GAGE RESPONSE

In the previous sections we have shown that determination of the resistance change of a gage element requires the knowledge of stresses and strains in the gage. The analyses in Section 3 were performed by assuming one stress component in the gage and by assuming a particular strain state in the gage. Although these assumptions are plausible, they are not rigorously justified. Also, they do not provide insight for a different loading situation, such as rotation of matrix stresses, as described in Section 4.1. Here we take a different approach: we determine the gage stresses and strains (hence resistance) by modeling the gage as an inclusion in a matrix and then solving the corresponding boundary value problem.

The analytic solutions presented are based on the Eshelby solution for an ellipsoidal elastic inclusion in an elastic matrix.[48] We have extended this solution to an elastic-plastic inclusion in an elastic matrix because the elastic inclusion solution is shown to be incorrect. Solutions for both loading and unloading have been obtained. Effects of gage aspect ratio on resistance change have also been examined. Before presenting the solutions, we discuss the applicability of the analysis to the experimental situation.

The experimental results given in Section 4.1 are used to check our theoretical analysis. In these experiments, the principal stresses in the matrix had different orientations with respect to the gage. We will, therefore, determine how well the present analysis can simulate the measured

resistance change ratios for the two different orientations. This simu-
lation is a better test of the theory than an absolute prediction for a
single orientation because the constants (α, β, and η in Section 2) are
not very accurately known. By comparing the ratios from two different
orientations, the accuracy requirements on the constants are somewhat
reduced. The use of experiments in Section 4.1 also ensures that the
matrix is elastic (although the inclusion may be plastic) as required
by our theoretical analysis.

The theoretical analysis ignores any dynamic effects such as scatter-
ing of the stress wave by the inclusion. We have assumed that the gage
is always in equilibrium with its surroundings. We are, therefore, solving
a static equilibrium problem for an imposed deformation in the matrix.

5.1 ELASTIC INCLUSION SOLUTION USING THE ESHELBY TECHNIQUE[*]

The solution to the general problem of the stress field determination
due to an elastic ellipsoidal inclusion in an elastic matrix was described
by Eshelby in 1957.[48] A brief discussion of the Eshelby technique and its
application to our experimental situation is given below.

Figure 5.1 shows an inclusion, bounded by a surface S, in an infinite
matrix. We wish to determine the stresses and strains in and around the
inclusion for a matrix strain imposed far away from the inclusion. Two
basic assumptions in Eshelby's work are: (1) linear elastic response for
the matrix and the inclusion, and (2) continuity of tractions and displace-
ments across the matrix-inclusion boundary; that is, the inclusion and
matrix are welded across the surface S. Eshelby's solution procedure is
based on an application of the Green's function in an elastic medium.
The solution consists of two parts and includes the steps indicated next.

---

[*]This work was done in collaboration with Prof. G. E. Duvall.

67
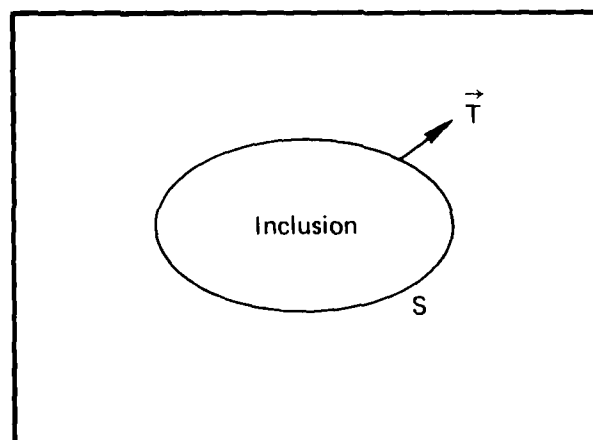
MA-8324-9

FIGURE 5.1   A SCHEMATIC VIEW OF AN INCLUSION BOUNDED BY A SURFACE
S IN A MATRIX

The traction vector normal to the surface is shown.

First, the transformation problem is solved. In this problem the 'inclusion' bounded by S is homogenous; that is, it is the same material as the matrix. The intent is to determine the elastic state of the matrix and the homogenous inclusion when only the inclusion is subjected to an arbitrary homogenous strain. The constraint provided by the remainder of the matrix gives rise to the stresses. In arriving at the solution of this problem, Eshelby considered the following hypothetical steps.

Make a cut along the boundary surface 'S' and impose the stress-free homogenous strain ϵ^T on the inclusion. The region bounded by S can no longer fit in the matrix and surface tractions $\vec{T}$ are needed to restore the strained inclusion to its original shape and size

$$\vec{T} = - \sigma^T \cdot \vec{N} \tag{5.1}$$

where $\sigma^T = H \cdot \epsilon^T$

H represents the elastic constants and $\vec{N}$ defines the normal to the surface S. If the inclusion (strain-free but not stress-free) is now put into the matrix (stress-free and strain-free) and welded across the surface S, then there is a body force of magnitude $\vec{T}$ spread over the surface S. To annul this force, impose a distribution $-\vec{T} = + \sigma^T \cdot \vec{N}$ on the surface S. This force produces a displacement field $\vec{u}^c (\vec{r})$. The stresses and strains in the matrix and inclusion can then be written using the elastic constants (λ and G).

$$
\text{Matrix}
\begin{cases}
\epsilon_{ij} = \epsilon^c_{ij} = 1/2 \left(\dfrac{\partial u^c_i}{\partial x_j} + \dfrac{\partial u^c_j}{\partial x_i} \right) \\[2em]
\sigma_{ij} = \sigma^c_{ij} = \lambda \epsilon^c_{mm} \delta_{ij} + 2G \epsilon^c_{ij}
\end{cases}
\tag{5.2}^*
$$

$$
\text{Inclusion}
\begin{cases}
\epsilon_{ij} = \epsilon^c_{ij} \\[2em]
\sigma_{ij} = \sigma^c_{ij} - \sigma^T_{ij}
\end{cases}
\tag{5.3}
$$

*Note, ϵ^c is a function of position.

69

The inclusion stress term takes into account the tractions that were required to bring the inclusion back to the original size and shape. Knowledge of u_i^c is the main step in determining the stresses and strains. Using the Green's function for an elastic medium, Eshelby derived the displacement field due to the forces $\sigma^T \cdot \vec{N}$ applied over the surface S, in terms of $\underset{\sim}{\sigma}^T$ and $\underset{\sim}{\epsilon}^T$, as follows:

$$u_i^c \; (\vec{X}) = \frac{\sigma_{jk}^T}{16\pi\mu(1-\nu)} \int \frac{dV}{r^2} \; f_{ijk} \; (\vec{\ell})$$

$$= \frac{\epsilon_{jk}^T}{8\pi(1-\nu)} \int \frac{dV}{r^2} \; g_{ijk} \; (\vec{\ell}) \qquad\qquad (5.4)$$

where
$$f_{ijk} = (1-2\nu) \; (\delta_{ij}\ell_k + \delta_{ik}\ell_j) - \delta_{jk}\ell_i + 3\ell_i\ell_j\ell_k$$

$$g_{ijk} = (1-2\nu) \; (\delta_{ij}\ell_k + \delta_{ik}\ell_j - \delta_{jk}\ell_i) + 3\ell_i\ell_j\ell_k$$

r and $\vec{\ell} = (\ell_1, \ell_2, \ell_3)$ are the length and direction of a line drawn from dV to the point of interest, and ν is Poisson's ratio. For an ellipsoidal inclusion, Eshelby showed that the above equations can be rewritten as

$$\epsilon_{ij}^c = S_{ijk\ell} \; \epsilon_{k\ell}^T \qquad\qquad (5.5)$$

where $S_{ijk\ell}$ depends only on the Poisson's ratio of the matrix and the shape of the ellipsoid.* Because $\epsilon_{k\ell}^T$ is uniform by definition, it follows that ϵ_{ij}^c is also uniform within the inclusion.

The solution of the transformation problem is used to solve the actual problem of interest: The inclusion and the matrix have different properties and an external strain ϵ^A is imposed at infinity. To solve this problem, replace the actual inhomogenous inclusion by an equivalent homogenous inclusion. The solution to this equivalent homogenous inclusion problem under external strain ϵ^A is obtained by superposing ϵ^A on the strain state of the inclusion and the matrix in the transformation problem.

---
*Although Equation (5.5) appears to be simple in form, the calculation of S is quite cumbersome.

Thus, the stresses in the 'equivalent inclusion' are

$$\underset{\sim}{\sigma}^{inc.} = \underset{\sim}{H} \cdot (\underset{\sim}{\varepsilon}^{C} + \underset{\sim}{\varepsilon}^{A} - \underset{\sim}{\varepsilon}^{T}) \tag{5.6}$$

In the actual inclusion (elastic constants H'), the strains $\underset{\sim}{\varepsilon}^{C} + \underset{\sim}{\varepsilon}^{A}$ give rise to a stress

$$\underset{\sim}{\sigma}^{inh.} = \underset{\sim}{H}' \cdot (\underset{\sim}{\varepsilon}^{C} + \underset{\sim}{\varepsilon}^{A}) \tag{5.7}$$

If $\sigma^{inc.} = \sigma^{inh.}$, then the equivalence with the homogenous inclusion is complete. We, therefore, write

$$\underset{\sim}{H}' \cdot (\underset{\sim}{\varepsilon}^{C} + \underset{\sim}{\varepsilon}^{A}) = \underset{\sim}{H} \cdot (\underset{\sim}{\varepsilon}^{C} + \underset{\sim}{\varepsilon}^{A} - \underset{\sim}{\varepsilon}^{T}) \tag{5.8}$$

where

$$\underset{\sim}{\varepsilon}^{C} = \underset{\sim}{S} \cdot \underset{\sim}{\varepsilon}^{T}$$

Equations (5.5) and (5.8) can be solved for $\underset{\sim}{\varepsilon}^{T}$ and $\underset{\sim}{\varepsilon}^{C}$ in terms of $\underset{\sim}{\varepsilon}^{A}$. For example, eliminating $\underset{\sim}{\varepsilon}^{C}$ between (5.5) and (5.8) gives

$$[(\underset{\sim}{H}' - \underset{\sim}{H}) \cdot \underset{\sim}{S} + \underset{\sim}{H}] \cdot \underset{\sim}{\varepsilon}^{T} = (\underset{\sim}{H} - \underset{\sim}{H}') \cdot \underset{\sim}{\varepsilon}^{A} \tag{5.9}$$

Solution of the simultaneous equations represented by Equation (5.9) give $\underset{\sim}{\varepsilon}^{T}$, which is then used to obtain $\underset{\sim}{\varepsilon}^{C}$ from Equation (5.5). Stresses in the matrix and the inhomogenous inclusion are determined from Equations (5.2) and (5.7), respectively. (In using Equation (5.2) it is necessary to add ε^{A} to ε^{C}).

In the experiments we are simulating, the gages were a rectangular parallel piped with dimensions: 2.5 cm by 0.2 cm by 0.005 cm. We make the following assumptions:

(1) For the times of interest, the gage length can be taken as infinite.

(2) The rectangular cross section 0.2 cm by 0.005 cm can be replaced by an elliptical cross section such that the area of the ellipse is the same as the rectangle (0.2 cm by 0.005 cm) and the axes have a ratio of 40 to 1.*

(3) Nonlinearities in elastic constants are ignored.

Because of the infinite length, we have a plane strain problem and the strain fields are as follows

$$\underset{\sim}{\varepsilon}^A = (\varepsilon_1^A, \varepsilon_2^A, \quad 0)$$

$$\underset{\sim}{\varepsilon}^C = (\varepsilon_1^C, \varepsilon_2^C, \quad 0)$$

$$\underset{\sim}{\varepsilon}^T = (\varepsilon_1^T, \varepsilon_2^T, \quad \varepsilon_3^T) \tag{5.10}$$

Note that $\underset{\sim}{\varepsilon}^T$ can have all three components non-zero in the theoretical formulation.[+] The stresses in the inclusion can be written as

$$\sigma_1 = (\lambda_1 + 2 G_1)(\varepsilon_1^C + \varepsilon_1^A) + \lambda_1 (\varepsilon_2^C + \varepsilon_2^A)$$

$$\sigma_2 = \lambda_1(\varepsilon_1^C + \varepsilon_1^A) + (\lambda_1 + 2 G_1)(\varepsilon_2^C + \varepsilon_2^A)$$

$$\sigma_3 = \lambda_1(\varepsilon_1^C + \varepsilon_1^A + \varepsilon_2^C + \varepsilon_2^A) \tag{5.11}$$

where λ_1 and G_1 are elastic constants for the inclusion.

In our experiments we are considering two cases:

Case I: The applied strain is one dimensional and along the gage thickness direction: ε_2^A. (The convention for the axes was given in Section 2.3).

Case II: The applied strain is one dimensional and along the gage width direction: ε_1^A.

----

*The semi-major and semi-minor axes are then 0.115 cm and 0.00287 cm, respectively.

[+] ε^T is a fitting parameter that matches the stresses in the actual and the equivalent inclusion.

72

The resistance change, ignoring the changes in stress-free resistivity,[*] can then be written as

Case I
$$\frac{\Delta R_3}{R_o} = \pi_{12}(\sigma_1 + \sigma_2) + \pi_{11}\sigma_3 - \epsilon_2^A - \epsilon_1^c - \epsilon_2^c \tag{5.12}$$

Case II
$$\frac{\Delta R_3}{R_o} = \pi_{12}(\sigma_1 + \sigma_2) + \pi_{11}\sigma_3 - \epsilon_1^A - \epsilon_1^c - \epsilon_2^c \tag{5.13}$$

We have used π_{ij} instead of α, β (see Eq. 2.7). The values for these constants were taken from the work of Grady and Ginsberg on Ytterbium gages.[30]

The procedure for evaluating $\Delta R/R_o$ in Equations (5.12) and (5.13) is as follows. ϵ^A is determined from experimental data on the matrix material.[†] Equation (5.9) is used to evaluate ϵ^T, and Equation (5.5) is then used to evaluate ϵ^c. These results are used to evaluate stresses in Equation (5.11). The stresses in conjunction with ϵ^A and ϵ^c give $\Delta R/R_o$. The ratio for the two cases is given as

$$\left(\frac{\Delta R_3}{R_o}\right)_{II} \bigg/ \left(\frac{\Delta R_3}{R_o}\right)_{I} = 2.1 \tag{5.14}$$

where we used the following elastic constants[**]

$$Yb: \quad K = 14.8 \text{ GPa}; \quad G = 7.25 \text{ GPa}$$
$$PMMA: \quad K = 6.02 \text{ GPA}; \quad G = 2.25 \text{ GPa}.$$

----

[*] This is the same as assuming $\eta = 0$ in Equation (2.12).

[†] The matrix material (PMMA) has been very well characterized under shock loading.[38]

[**] The constants for Yb are taken from Reference 30. PMMA constants are taken from Reference 39 and reflect the moduli appropriate at high strain rates.

73

The above result is clearly in error, because the experimental
measurements give a value of 0.64 ± 0.06. Examination of the various
steps in the calculation showed that the large difference in the theory
and experiment could not be ascribed to errors in constants. The main
error was due to the large stresses resulting from the stress concentration
in Case II. (The stresses and strains for these calculations are discussed
in the next subsection.) These concentrations are a consequence of the
aspect ratio. Simple buckling calculations showed that elastic buckling
could not occur for our problem and, therefore, could not explain our
experimental results.

The difficulty with our stress solution is that it does not account
for gage plasticity. The incorporation of plasticity should dramatically
alter the stresses because the stress differences have to satisfy the
yield condition. The extension of the solution to an elastic-plastic
inclusion is considered in the next subsection.

5.2 MODELING THE GAGE AS AN ELASTIC-PLASTIC INCLUSION

The Eshelby solution can be extended to an elastic-plastic inclusion,
as described below, and the results can then be used to calculate the
resistance change for the two orientations.

In the Eshelby solution for an elastic inclusion, the inhomogenous
inclusion can be replaced by an equivalent homogenous inclusion provided
we satisfy the stress equivalence in Equation (5.8).

$$H' \cdot (\epsilon^C + \epsilon^A) = H \cdot (\epsilon^C + \epsilon^A - \epsilon^T)$$

The right-hand side is the stress in the equivalent inclusion and H refers
to the matrix elastic constants. The left-hand side is the stress in the
actual inclusion. For an elastic inclusion, H' are elastic constants.
In general, however, there is nothing in the theoretical formalism that
restricts the form of the left-hand side provided the stress equivalence
is satisfied.[49] We can therefore choose any constitutive relation for the
inclusion. Another way of explaining this result is as follows: The
strains developed in the actual inclusion are such that the constitutive

74

relation for the inclusion and stress equality with the equivalent
inclusion are simultaneously satisfied. To avoid confusion, we rewrite
Equation (5.8) as

$$H'' \cdot (\varepsilon^C + \varepsilon^A) = H \cdot (\varepsilon^C + \varepsilon^A - \varepsilon^T) \qquad (5.15)$$

The tensor H'' no longer represents the elastic constants. Instead, it
relates the stresses and strains of an elastic-plastic body.

The constitutive model used for the gage is the same as that presented
in Section 2.2. The elastic constants for the PMMA and Yb are taken to
be linear with the same values as in the previous calculation. The yield
function for the Yb is a von-Mises yield law expressed as

$$\sqrt{J_2'} - Y_o = 0 \qquad (5.16)$$

where Y_o is taken to be 0.45 kbar. Because of a lack of existing data,
work-hardening is not included. The calculations are carried out
incrementally in 100 steps to a peak strain of 5.9% (corresponding to
experiments in Section 4.1). The procedure consists of performing an
elastic calculation until the onset of yield.[*] On yielding, the
increment is further subdivided to accurately obtain the matrix strain
corresponding to yielding. On yielding, the modulus tensor is redefined
and the appropriate stresses are obtained. The procedures during loading
and unloading are similar; that is, each incremental calculation is first
performed elastically and if yielding occurs, it is taken into account.

The results of the resistance change calculation as a function of
matrix strain for the two orientations are shown in Figure 5.2. For
comparison with our experiments, only the peak values are of interest.

----

[*]The total stresses and strains at any instant are obtained by adding
the increments to the previous value.
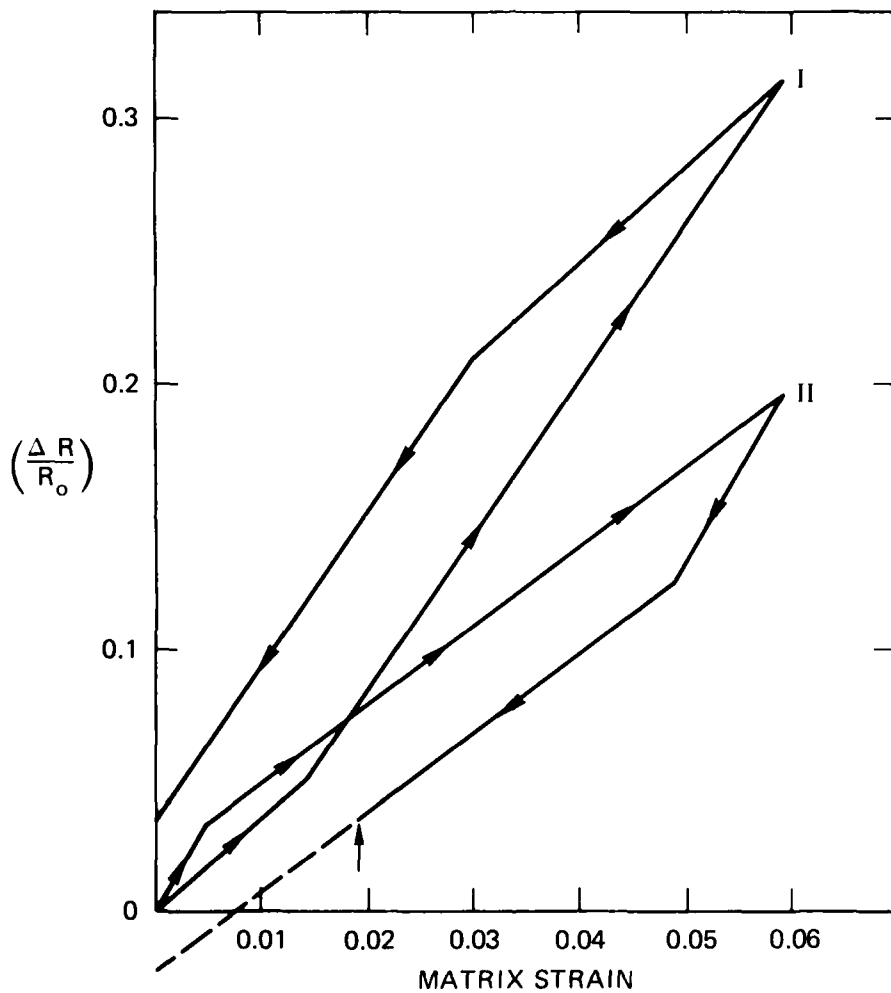
FIGURE 5.2 CALCULATED RESISTANCE CHANGE OF Yb GAGES (MODELED AS ELASTIC-, LASTIC INCLUSIONS) VERSUS MATRIX STRAIN

The response shown in this figure is for gages with major surface normal to shock propagation direction (I) and major surface parallel to shock propagation direction (II).

76

The calculated ratio at peak strain is

$$\left(\frac{\Delta R}{R_o}\right)_{II} \Big/ \left(\frac{\Delta R}{R_o}\right)_{I} = 0.63 \tag{5.17}$$

This result is in good agreement with the measured resistance change ratio (0.64 ± 0.06). We emphasize that the closeness in the agreement is fortuitous because the constants are not very well known.[*] The main result of this calculation is that by modeling the gage as an elastic-plastic inclusion, we can predict the resistance change reasonably well and can, therefore, understand the gage response.

Further discussion of the resistance change calculations (Figure 5.2) will be presented after an examination of stresses and strains in the gage. Table 5.1 lists the stresses and strains in the inclusion (gage) and in the matrix (far from the inclusion). For the gage, we have also shown, in parenthesis, the stresses and strains for the elastic inclusion solution. In Case I, the stress normal to the major surface of the gage (inclusion) is equal to the matrix stress in that direction,[+] with the other stresses for the plastic case being determined by the yield condition. The gage strain state, though different from the matrix strain state, is largely uniaxial ($\varepsilon_2/\varepsilon_1$ = 28.3). The strain along the X_1 direction is a consequence of two competing effects: the large aspect ratio of the inclusion that tends to reduce it, and differences in the mechanical impedance between the inclusion and the matrix that tend to increase it. The elastic solution for Case I shows an identical normal stress, but the other stresses are considerably smaller in comparison to the plastic solution. The inclusion strains are also smaller for the elastic case. Thus, the elastic solution gives a lower $\Delta R/R_o$ for this orientation.

---

[*] In fact, the individual resistance change values differ by about 10%.

[+] This calculation rigorously proves the assumption that the normal stress is the same in the gage and the matrix.

Table 5.1

STRESSES AND STRAINS IN THE MATRIX AND THE GAGE[*]

Case	Direction[†]	Matrix Stress (kbar)	Matrix Strain (%)	Gage Stress (kbar)	Gage Strain (%)
I	X_1	-2.68[‡]	0	-4.61 (-2.29)	0.12 (-0.05)
	X_2	-5.34	-5.92	-5.38 (-5.37)	-3.4 (-2.17)
	X_3	-2.68[‡]	0	-4.59 (-2.22)	0
II	X_1	-5.34	-5.92	-3.54 (-12.24)	-6.07 (-5.55)
	X_2	-2.68[‡]	0	-2.7 (-2.73)	4.04 (1.1)
	X_3	-2.68[‡]	0	-2.84 (4.33)	0

[*] Tensile stresses and strains are considered positive. The values in the parenthesis refer to the elastic inclusion solution discussed in Subsection 5.1.

[†] These directions refer to the gage: Length is along X_3, width along X_1, and thickness along X_2.

[‡] The use of nonlinear elastic constants will give the correct value: 3.05 kbar.

For Case II, the stress normal to the major surface of the inclusion is again equal to the matrix stress in that direction. The other stresses (determined by the yield condition) are no longer equal because of the stress concentration effect due to gage geometry. The strain states for this case are quite complex, with compression in one direction and tension along the other. For the elastic solution, the strains are smaller, but they have the same sign as the plastic solution. The stresses, on the other hand, are very large due to stress concentration and give rise to a large resistance change for this orientation. The large stress values are responsible for the incorrect ratio obtained in Section 5.1. The development of tensile strains in Case II is an interesting result that should be examined experimentally.

The above results show that the stresses along the normal to the foil are equal to the matrix stresses because of the large aspect ratio (40 to 1) of the foil. The strains, on the other hand, cannot be predicted as easily. In the experimental situations considered here (uniaxial strain in the matrix), the contribution of the strains is quite small and the stresses dominate the resistance change. This is not true in general.

The plot shown in Figure 5.2 (resistance change versus strain) is the plot that would be generated by a series of experiments having different matrix strains. It is important to note that yielding for the two orientations occurs at different matrix strains. In the elastic range, the resistance change for Case II is higher than in Case I. This result is contrary to a simple empirical usage of the gage and needs to be examined by experiments in the low strain range. The straight line form of the results is a consequence of ignoring the nonlinear material properties. On unloading, the usual orientation (Case I) gives rise to hysteresis. This hysteresis is purely due to non-zero stresses and strains in the gage because changes in stress-free resistivity have not been considered in our calculation. The unloading for Case II is more complex and the arrow marks the spot where one of the gage stresses becomes tensile. The resistance change results below that strain level are probably not realistic because the foil may separate from the matrix. More work is needed to better understand the solutions for unloading in Case II.

79

We can also use this analysis to examine the effect of gage aspect ratio (width-to-thickness ratio) on the gage response. To compare the output of the wire gages with foil gages we performed the calculations for a circular cross section. The calculations were done for Yb., keeping all other gage and matrix variables the same as the elliptic cross section. For the circular inclusion, there is no effect of matrix stress rotation (as expected), and we obtained a value of $(\Delta R/R_o) = 0.29$. The resistance change for the elliptic inclusion (Case I) was 0.32. We can therefore conclude that the wire gage would show a lower resistance change in contrast to the foil gage.

The results for Manganin are expected to be similar and should qualitatively explain the lower value of Lee's[17] results in comparison with the results of Barsis et al.[18] as discussed in Section 3.1.

5.3 SUMMARY

By modeling the gage as an elastic-plastic inclusion* and using the phenomenological model developed in Section 2, we can predict the response of piezoresistance gages. The results from the analysis presented in this section can be summarized as follows:

- The changes in the gage response to rotations in the stress components in the matrix were correctly predicted.

- The simple empirical relation used for piezoresistance gage calibration under shock loading is shown to be a consequence of the gage plasticity and the gage-matrix interaction.

- The theoretical basis for developing a lateral stress gage has been presented. Further work needs to be done to understand the unloading response of a gage used for lateral stress measurements.

- For the experimental situations considered, the total strain (or dimensional) contribution to resistance change has been shown to be small.

- The present analysis permits an assessment of the foil aspect ratio on the gage response.

---

*We remind the reader that the assumption of displacement continuity at the inclusion-matrix boundary is inherent in the analysis. Although this assumption is quite restrictive, the state of matrix strain coupled with gage plasticity reduces its importance for our work.

SECTION 6

DISCUSSION AND RECOMMENDATIONS

The analysis presented in the Section 5 completes our solution
to the direct problem; that is, we have successfully modeled the gage
response to an imposed matrix deformation. The results show that the
important variables in understanding the gage response are gage plasti-
city and the gage-matrix interaction. This latter variable takes into
account matrix strain and gage shape. In this section we first discuss
the various assumptions made in our gage-matrix interaction analysis.
Next, we examine the implications of our results to the measurement of
stress in a complex loading situration, namely, divergent flow.

We assumed the gage length to be infinite in our calculations.
This assumption is not necessary for solving the problem and is made to
facilitate the calculations (determination of S in Eq. 5.5.). The
assumption is reasonable given the length-to-thickness ratio (500 to 1)
and the times of interest in shock wave measurements. For a truly static
problem, the effect of finite length needs to be examined.

The gage cross section is taken to be elliptical in our calculations.
There are two potential difficulties with this assumption: (1) Initially,
the gage has a rectangular cross section, and (2) the effect of the stress
wave on the gage shape is not considered. Replacing the rectangular
cross section by an elliptic cross section seemed reasonable for the large
aspect ratio of our work (40 to 1). To rigorously examine the validity
of this assumption, finite element calculations[*] were performed with an
elliptical and a rectangular cross section. Except for the edges along
the larger dimension,[†] the stresses in the inclusion were the same for

---

[*] These were performed by Dr. L. Schwer of SRI using the NONSAP code.[50]

[†] There were 160 elements along the larger dimension and only the 5
elements on each end showed significant derivations.

81

the two cases. The results of these calculations justified our use of the elliptical inclusion. The distortion at the edges is not considered important because of the stress wave effect discussed below.

Using a static boundary value analysis for a dynamic problem ignores the distortion to the gage shape due to the incident shock wave.[*] Hence, the exact shape of the gage after the shock wave has traversed over the specimen is not known. Although we do not believe this effect would make a large contribution, we can neither prove or justify this statement. Future work should attempt to determine the contribution from gage distortion.

The results from our work show the difficulty in inverting gage data (a scalar measurement) from an arbitrary loading situation. In fact, it is reasonable to say that the resistance change data, without knowledge of some other parameters, would be impossible to analyze. This then brings up the question: How can piezoresistance gages be used in more complex situations, such as diverent loading? To make such measurements, two aspects of the problem must be addressed: Determination of the gage constants (α, β, η) indicated in Section 2, and examination of the gage package-matrix interaction.

A determination of the gage constants is necessary to interpret the gage data. If the constants are known, then the gage calibration is more general and we do not have the difficulties encountered in analyzing the data of Section 4.1. This determination requires gage measurements for several strain paths in the matrix. If the stresses are low enough, then the gage responds elastically, and this permits determination of α and β. Plastic deformation of the gage and relating the plastic work to change in the stress-free resistivity can provide η. This latter measurement, though not simple, needs to be attempted for at least one gage type to complete our understanding of piezoresistance gages.

[*] This was pointed out by Dr. M. Cowperthwaite.

82

The other aspect of the problem concerns gage-matrix interaction
for the specific loading situation. To use these gages effectively, one
must know the state of strain in the matrix and have some idea of the
matrix response. Analyses can then be performed to determine the gage
response sensitivity to various matrix material property parameters.
Such calculations can provide the optimal gage package shape and determine
the parameter that dominates the gage response. For example, in the uni-
axial strain experiments discussed in this report, the dimensional
terms had negligible contribution. For divergent flow, this is not true
and the contribution of the dimensional changes needs to be assessed.
How effectively a nonpiezoresistive material can be used to assess strains
in the gage itself can also be examined by performing a gage matrix
interaction analysis.*

The gage matrix interaction analysis is also important for evaluating
the effect of the gage package on the matrix stresses in the vicinity of
the gage. The presence of the gage can induce yielding or other re-
arrangement of stresses near the gage.

In conclusion, piezoresistance gages can be used in complex loading
situations provided gage constants are evaluated and gage matrix inter-
action analyses are performed to ensure that the measurements can indeed
be inverted to determine the stresses of interest. Similar remarks apply
to the development of strain-compensated gage packages.

*Also see discussion at the end of Section 2.

BLANK PAGE

APPENDIX A

ELASTIC-PLASTIC RELATIONS

In this appendix, we derive the equations relating stresses and strains that are used in Section 3. The elastic-plastic model used in deriving these equations is presented in Section 2.2. The relations presented here are for 1- and 2-strain states in the material (assuming small strain). A detailed discussion of elastic-plastic relations for 1-D strain is given in the paper by Fowles.[51]

One-Dimensional Strain ($\epsilon_x \neq 0$, $\epsilon_y = \epsilon_z = 0$)

This strain configuration has been extensively studied in shock wave studies. In the elastic region, we have the stresses

$$\sigma_x = (\lambda + 2\mu)\epsilon_x^e$$

$$\sigma_y = \sigma_z = \lambda\epsilon_x^e \qquad (A.1)$$

Using the von Mises yield condition, we can write the compressive stress at yield as[*]

$$p_x^{HEL} = Y^o \left(\frac{1 - \nu}{1 - 2\nu} \right) \qquad (A.2)$$

where λ, μ, and ν are elastic constants; Y^o is yield stress in simple tension; and p_x^{HEL} is the Hugoniot elastic limit. Beyond the elastic limit

$$P_x - P = \frac{2}{3} Y \qquad (A.3)$$

where P is the mean compressive stress and Y is yield stress in simple tension. Thus, in the plastic range the compressive stress σ_x is offset by 2Y/3 from the hydrostat. For perfectly plastic solid, $Y = Y^o$.

[*] P's denote compressive stress as positive.

Two-Dimensional Strain ($\epsilon_x = \epsilon_y \neq 0$, $\epsilon_z = 0$)

For this strain configuration, we have the stresses

$$\sigma_x = \lambda(\epsilon_x^e + \epsilon_y^e) + 2\mu\epsilon_x^e$$

$$\sigma_y = \lambda(\epsilon_x^e + \epsilon_y^e) + 2\mu\epsilon_y^e \qquad (A.4)$$

$$\sigma_z = \lambda(\epsilon_x^e + \epsilon_y^e)$$

Combining the above equations, we obtain

$$\sigma_x - \frac{\sigma_{mm}}{3} = \frac{\sigma_x - \sigma_z}{3} \qquad (A.5)$$

and

$$\sigma_x = \frac{\lambda + \mu}{\mu} (\sigma_x - \sigma_z) \qquad (A.6)$$

Using the von Mises condition, we have at the yield point

$$P_x^{HEL} = \left(\frac{1}{1-2\nu}\right) Y^o \qquad (A.7)$$

and

$$P_x - P = \frac{1}{3} Y^o \qquad (A.8)$$

Here the P_x^{HEL} corresponds to the compressive stress at yield for the two-dimensional strain configuration. Y represents yield stress in simple tension. By eliminating ν between Equations (A.2) and (A.7), we obtain

$$P_{xo}^{2D} = 2P_{xo}^{1D} - Y^o \qquad (A.9)$$

where P_{xo}^{2D} = compressive stress at yield in a two-dimensional configuration.

P_{xo}^{1D} = compressive stress at yield in a one-dimensional configuration.

Equation (A.9) gives the compressive stress at yield for two-dimensional strain. Because $P_{xo}^{1D} > Y^o$, the HEL in two-dimensional strain is higher than that in one-dimensional strain. The offset between the mean stress and P_x is $Y/3$--that is, half of the offset observed in the one-dimensional strain.

Using the equations presented in this appendix, we can compute the mean stress or pressure corresponding to a compressive stress for the one- or two-dimensional strain configuration.

BLANK PAGE

APPENDIX B

DIMENSIONAL TERM FOR SIMPLE LOAD PATHS

The dimensional term in Equation (2.12) can be expressed in terms of density changes using the small strain approximation. The trace of the strain tensor is expressed as[*]

$$\epsilon_{mm} = \rho_o/\rho - 1 \tag{B.1}$$

Hydrostatic Loading ($\epsilon_{11} = \epsilon_{22} = \epsilon_{33}$)

$$\frac{1 + \epsilon_{11}}{(1 + \epsilon_{22})(1 + \epsilon_{33})} = \frac{1}{\left(1 + \dfrac{\epsilon_{mm}}{3}\right)} \approx 1 - \frac{\epsilon_{mm}}{3} \tag{B.2}$$

$$(\rho_H/\rho_o)^{1/3} = (1 + \epsilon_{mm})^{-1/3} \approx 1 - \frac{\epsilon_{mm}}{3} \tag{B.3}$$

The equivalence of (B.2) and (B.3) allow the dimensional term for hydrostatic loading to be expressed as $(\rho_H/\rho_o)^{1/3}$

One-Dimensional Strain ($\epsilon_{11} = \epsilon_{33} = 0$, $\epsilon_{22} \neq 0$)

$$\frac{1 + \epsilon_{11}}{(1 + \epsilon_{22})(1 + \epsilon_{33})} = \frac{1}{1 + \epsilon_{mm}} = \rho_{1D}/\rho_o \tag{B.4}$$

Two-Dimensional Strain ($\epsilon_{11} = \epsilon_{22} \neq 0$, $\epsilon_{33} = 0$)

$$\frac{1 + \epsilon_{11}}{(1 + \epsilon_{22})(1 + \epsilon_{33})} \cdot \frac{1}{1 + \epsilon_{mm}} = \rho_{2D}/\rho_o \tag{B.5}$$

In Equations (B.3) through (B.5), the density in the strained material refers to the density for that particular loading.

---

[*] This is using an Eulerian strain measure and noting that strain is positive in tension.

BLANK PAGE

APPENDIX C
RESIDUAL RESISTANCE UPON LONGITUDINAL UNLOADING

Presented below are the equations needed to compute the residual resistance upon longitudinal unloading from a plastic state. The relations are for one- and two-dimensional strain states and use the small strain approximation.

The residual resistance change can be computed using Equation (3.4) in Section 3.

$$\frac{\Delta R_3}{R_o} = \pi_{3n}\, \sigma_n \;+\; G_{3m}\, \epsilon_m \tag{C.1}$$

For uniaxial strain loading ($\epsilon_1 \neq 0$, $\epsilon_2 = \epsilon_3 = 0$), Equation (C.1) upon longitudinal unloading becomes

$$\left(\frac{\Delta R_3}{R_o}\right)^{1D}_{Res.} = \pi_{12}\, \sigma_2 \;+\; \pi_{11}\sigma_3 - \epsilon_1 \tag{C.2}$$

For two-dimensional strain ($\epsilon_1 = \epsilon_2 \neq 0$, $\epsilon_3 = 0$), Equation (C.1) upon longitudinal unloading becomes

$$\left(\frac{\Delta R_3}{R_o}\right)^{2D}_{Res.} = \pi_{11}\, \sigma_3 - (\epsilon_1 + \epsilon_2) \tag{C.3}$$

The stresses and strains appearing in Equations (C.2) and (C.3) are determined from the elastic-plastic relations present in Appendix A. A graphical representation for the loading and unloading paths is shown in Figure C.1.[*] Various stress components as a function of volume strain for one- and two-dimensional strain have been shown and are explained next.

---

[*] The curves shown are for Yb.
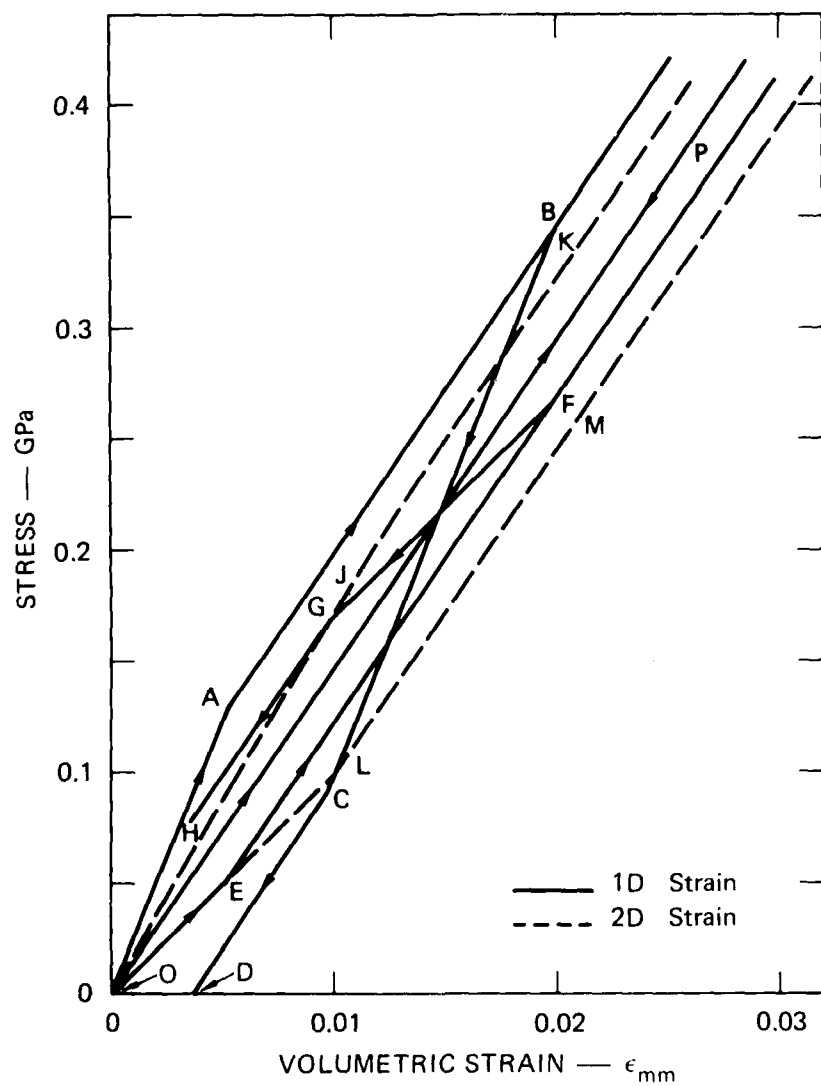
FIGURE C.1   ELASTIC-PLASTIC MECHANICAL RESPONSE OF Yb
FOR 1D AND 2D STRAINS

For one-dimensional strain loading, OABCD represents the longitudinal stress-strain path. Points A and C mark the onset of yielding. The lateral stress-strain path corresponding to OABCD is marked as OEFGH where the prints E and G mark the onset of yielding. The line OP represents the mean stress-strain path. By writing algebraic equations for these lines, we can calculate the non-zero stresses and strains upon longitudinal unloading.

For two-dimensional strain, we have shown only the loading path to simplify the figure. OJK represents the longitudinal stress-strain curve and OLM represents the path for the other stress. Strains corresponding to J and L mark the onset of yielding. The mean stress-strain curve stays the same as that for one-dimensional strain. As shown in Appendix A, the yielding under two-dimensional strain occurs at a different strain level, and the longitudinal stress offsets from the mean stress-strain curve are smaller.

For an elastic-perfectly plastic solid, above a threshold strain the residual stresses and strains are constant because the stresses upon longitudinal unloading are limited by the yield stress. The calculations performed here consisted of evaluating the threshold strain for one- and two-dimensional loading. Below the threshold strain, a linear relationship can be used to evaluate the residual stresses.

93

BLANK PAGE

REFERENCES

1. R. A. Shunk, "Ground Motion Instrumentation Specification Below One Kilobar," Defense Nuclear Agency, Report DNA 3431F (1975).

2. D. R. Grine and P. L. Coleman, "Ground Motion Gage Development," Defense Nuclear Agency, Report DNA 3524T (1974).

3. D. D. Keough, presentation at the Defense Nuclear Agency Strategic Structures Division Biennial Review Conference held at SRI International (1979).

4. P. S. DeCarli, R. T. Bly, and J. T. Rosenberg, "Stress and Ablation Measurements on Hybla Gold," Draft Final Report, Contract No. DNA-001-77-C-0161, August 1978.

5. P. S. De Carli, work on DNA Contract DNA001-80-C-0142, SRI International, Menlo Park, California (1980).

6. P. W. Bridgeman, Proc. Am. Acad. Arts. Sci. 47, 321 (1911); see reference to work by E. Lisell in this paper.

7. P. W. Bridgeman, "The Effect of Homogeneous Mechanical Stress on the Electrical Resistance of Crystals," Phys. Rev. 42, 858 (1932).

8. P. W. Bridgeman, The Physics of High Pressure (G. Bell and Sons Ltd., London, 1958).

9. C. S. Smith, "Piezoresistance Effect in Germanium and Silicon," Phys. Rev. 94. 42 (1954).

10. R. W. Keyes, "The Effect of Elastic Deformation on the Electrical Conductivity of Semiconductors," in Solid State Physics (Academic Press, New York, 1960), Vol. II.

11. The work by Hauver is described in "Shock Waves" in High Pressure Physics and Chemistry, R. S. Bradley, Ed. (Academic Press, New York, 1963), Vol. 2, p. 250.

12. P.J.A. Fuller and J. H. Price, Brit. J. Appl. Phys. 15, 751 (1964).

13. D. Bernstein and D. D. Keough, J. Appl. Phys. 35, 1371 (1964).

14. D. D. Keough, "Procedure for Fabrication and Operation of Manganin Shock Pressure Gages," Final Report, Contract AF29(601)-68-C-0038, Technical Report No. AFWL-TR-68-57, Stanford Research Institute, Menlo Park, California (August 1968).

15. J. W. Lyle, R. L. Schreiver and A. R. McMillan, J. Appl. Phys. 46, 4663 (1969).

16. D. D. Keough and J. Y. Wong, J. Appl. Phys. 41, 3508 (1970).

17. E. Barsis, E. Williams, and C. Skoog, J. Appl. Phys. 41, 5155 (1970).

18. L. M. Lee, J. Appl. Phys. 44, 4017 (1973).

19. P. S. DeCarli, "Stress-Gage System for the Megabar (100 GPa) Range," Defense Nuclear Agency, Final Report 4066F (1976).

20. D. D. Keough, "Development of a High-Sensitivity Piezoresistive Stress Transducer for the Low Kilobar Range," Final Report, Contract No. DASA01-69-C-0014, SRI Internaitonal, Menlo Park, California (1970).

21. M. J. Ginsberg et al., "Effects of Stress on the Electrical Resistance of Ytterbium and Calibration of Ytterbium Stress Transducers," Final Report Contract DNA001-72-C-0146, SRI International, Menlo Park, CA (1973).

22. R. R. Horning and W. M. Isbell, Rev. Sci. Instr. 46, 1374 (1975).

23. P. Krehl, Rev. Sci. Instr. 49, 1477 (1978).

24. M. Perez and P. Chartagnac, Rev. Sci. Instr. 51, 921 (1980).

25. R. F. Williams and D. D. Keough, Bull. Amer. Phys. Soc. 12, 1127 (1967).

26. J. T. Rosenberg, "Development of a Piezoresistant Transducer to Measure Stress-Time Output of Small Detonators," AD-912487L, Picatinny Arsenal, Dover, New Jersey (1973).

27. W. P. Mason, Crystal Physics of Interaction Processes, (Academi Press, New York, 1966), Chap. 10.

28. J. T. Rosenberg and M. J. Ginsberg, Bull. Am. Phys. Soc. Series II, 17, 1099 (1972).

29. J. J. Dick and D. L. Styris, J. Appl. Phys. 46, 1602 (1975).

30. D. E. Grady and M. J. Ginsberg, J. Appl. Phys. 48, 2179 (1977).

31. D. J. Steinberg and D. L. Banner, J. Appl. Phys. 50, 235 (1979).

32. H. C. Vantine, L. M. Erickson, and J. A. Janzen, J. Appl. Phys. 51, 1957 (1980).

33. W. P. Mason and R. N. Thurston, J. Acoust. Soc. Amer. 29, 1096 (1957).

34. Y. C. Fung, Foundations of Solid Mechanics (Prentice-Hall, Inc., New Jersey, 1965).

35. J. A. Charest, "Development of a Strain-Compensated Shock Pressure Gauge," Report submitted by Dynasen, Inc., to Los Alamos Scientific Laboratory, Goleta, California (1979).

36. E. M. Lilley and D. R. Stephens, "Electrical Resistance of Ytterbium as a Function of Temperature and Pressure," UCRL-51006, Lawrence Radiation Laboratory, Livermore, CA (1971).

37. D. R. Stephens, J. Phys. Chem. Solids, 25, 423 (1964).

38. L. M. Barker and R. E. Hollenbach, J. Appl. Phys. 41, 4208 (1970).

39. Y. M. Gupta, "Determination of the Impact Response of PMMA using Combined Compression and Shear Waves," paper to be published in J. Appl. Phys. (1980).

40. This gas-gun is identical to that described in the paper by G. R. Fowles et al., Rev. Sci. Instr. 41, 984 (1970).

41. Y. M. Gupta et al., Rev. Sci. Instr. 51, 183 (1980).

42. G. R. Fowles and R. F. Williams, J. Appl. Phys. 41, 360 (1970).

43. D. Bernstein, C. Godfrey, A. Klein, and W. Shimmin, in Behavior of Dense Media Under High Dynamic Pressures (Gorden and Breach, New York, 1968), p. 461.

44. T. F. Stubbs, K. D. Seifert, and R. P. Swift, "Direct Observation of Transverse Stresses: The Tangential Stress Gage," Final Report to Advanced Research Projects Agency under Contract No. H0220014, Physics International Company, San Leandro, CA 94577 (1973)

45. G. I. Kanel, A. M. Molodets, and A. N. Dremin, Combustion, Explosion and Shock Waves 13, 772 (1978); translated from Fizika Goreniya i Vzryva, 13, 906 (1977).

46. C. V. Cagle, Handbook of Adhesive Bonding (McGraw-Hill, N.Y. 1973), p. 19-4.

47. Y. M. Gupta et al., Rev. Sci. Instr. 51, 183 (1980).

48. J. D. Eshelby, Proc. Royal Soc. London, A, 241, 376 (1957).

49. Discussions with Professors J. Rudnicki (University of Illinois) and D. Barnett (Stanford University) on the Eshelby formulation at the 14th Engineering Science Meeting held at Northwestern University (October 1979) are gratefully acknowledged.

50. K. J. Bathe, E. L. Wilson, and R. M. Iding, "NONSAP, A Structural Analysis Program for Static and Dynamic Problems of Nonlinear Systems, Univ. of California Structural Engineering Laboratory Report No. UC-SESM 74-3, Berkeley, CA (1974).

51. G. R. Fowles, J. Appl. Phys. 32, 1475 (1961).

BLANK PAGE

DISTRIBUTION LIST

DEPARTMENT OF DEFENSE

Assistant to the Secretary of Defense
Atomic Energy
    ATTN: Executive Assistant

Defense Nuclear Agency
    ATTN: SPTD
2 cy ATTN: SPSS
4 cy ATTN: TITL

Defense Technical Information Center
12 cy ATTN: DD

Field Command
Defense Nuclear Agency
    ATTN: FCPR
    ATTN: FCTMOF
    ATTN: FCT

Field Command
Defense Nuclear Agency
Livermore Branch
    ATTN: FCPRL

NATO School (SHAPE)
    ATTN: U.S. Documents Officer

Under Secretary of Defense for Rsch & Engrg
    ATTN: Stratetic & Space Sys (OS)

DEPARTMENT OF THE ARMY

Harry Diamond Laboratories
Department of the Army
    ATTN: 00100 Commander/Tech Dir/TSO
    ATTN: DELHD-N-P

U.S. Army Ballistic Research Labs
    ATTN: DRDAR-BLT, J. Keefer
    ATTN: DRDAR-BLV
    ATTN: DRDAR-TSB-S

U.S. Army Chemical School
    ATTN: ATZN-CM-CS

U.S. Army Cold Region Res Engr Lab
    ATTN: CRREL-EM

U.S. Army Engr Waterways Exper Station
    ATTN: F. Hanes
    ATTN: J. Ingram
    ATTN: Library
    ATTN: WESSA, W. Flathau
    ATTN: WESSE, L. Ingram

U.S. Army Materiel Dev & Readiness Cmd
    ATTN: DRXAM-TL

U.S. Army Nuclear & Chemical Agency
    ATTN: Library

DEPARTMENT OF THE NAVY

David Taylor Naval Ship R&D Ctr
    ATTN: Code L42-3
    ATTN: Code 1770

DEPARTMENT OF THE NAVY (Continued)

Naval Civil Engineering Laboratory
    ATTN: Code L08A

Naval Surface Weapons Center
    ATTN: Code F31

DEPARTMENT OF THE AIR FORCE

Air Force Institute of Technology
    ATTN: Library

Air Force Weapons Laboratory
Air Force Systems Command
    ATTN: DEX
    ATTN: NTE, M. Plamondon
    ATTN: DEX, J. Renick
    ATTN: SUL

Air University Library
Department of the Air Force
    ATTN: AUL-LSE

Assistant Chief of Staff
Intelligence
Department of the Air Force
    ATTN: INT

DEPARTMENT OF ENERGY

Department of Energy
Albuquerque Operations Office
    ATTN: CTID

Department of Energy
Nevada Operations Office
    ATTN: Mail & Records for Tech Lib

OTHER GOVERNMENT AGENCIES

Central Intelligence Agency
    ATTN: OSWR/NED

Department of the Interior
U.S. Geological Survey
    ATTN: D. Roddy

Federal Emergency Management Agency
    ATTN: Asst Dir for Rsch, J. Buchanon

DEPARTMENT OF ENERGY CONTRACTORS

Lawrence Livermore National Lab
    ATTN: Technical Info Dept Library

Los Alamos National Scientific Lab
    ATTN: MS 670, J. Hopkins

Oak Ridge National Laboratory
    ATTN: Civ Def Res Proj, Mr. Kearny

Sandia National Laboratories
    ATTN: Lib & Sec Class Div

DEPARTMENT OF ENERGY CONTRACTORS (Continued)

Sandia National Lab
    ATTN: L. Vortman
    ATTN: 3141
    ATTN: A. Chaban

DEPARTMENT OF DEFENSE CONTRACTORS

Acurex Corp
    ATTN: K. Triebes

Aerospace Corp
    ATTN: Tech Info Svcs
    ATTN: P. Mathur

Agbabian Associates
    ATTN: M. Agbabian

Artec Associates, Inc
    ATTN: D. Baum

BDM Corp
    ATTN: T. Neighbors
    ATTN: Corporate Library

Boeing Co
    ATTN: Aerospace Library
    ATTN: B. Lempriere

California Research & Technology, Inc
    ATTN: K. Kreyenhagen

Develco, Inc
    ATTN: L. Rorden

Effects Technology, Inc
    ATTN: R. Parisse

EG&G Wash Analytical Svcs Ctr, Inc
    ATTN: Library

Electromech Sys of New Mexico, Inc
    ATTN: R. Shunk

Eric H. Wang
Civil Engineering Rsch Fac
    ATTN: N. Baum

Geocenters, Inc
    ATTN: L. Isaacson

H-Tech Labs, Inc
    ATTN: B. Hartenbaum

Horizons Technology, Inc
    ATTN: R. Kruger

IIT Research Institute
    ATTN: Documents Library

J. D. Haltiwanger Consult Eng Svcs
    ATTN: W. Hall

Kaman Sciences Corp
    ATTN: Library
    ATTN: D. Sachs

Kaman Tempo
    ATTN: J. Shoutens
    ATTN: DASIAC

DEPARTMENT OF DEFENSE CONTRACTORS (Continued)

Merritt CASES, Inc
    ATTN: J. Merritt
    ATTN: Library

Pacific-Sierra Research Corp
    ATTN: H. Brode

Physics Applications, Inc
    ATTN: C. Vincent

Physics International Co
    ATTN: F. Sauer
    ATTN: Technical Library

R & D Associates
    ATTN: Tech Info Cntr
    ATTN: J. Lewis
    ATTN: P. Haas

Science Applications, Inc
    ATTN: J. Dishon

Science Applications, Inc
    ATTN: Technical Library

Science Applications, Inc
    ATTN: W. Layson
    ATTN: B. Chambers III

Science Applications, Inc
    ATTN: K. Sites

Southwest Research Institute
    ATTN: A. Wenzel
    ATTN: W. Baker

SRI International
    ATTN: B. Gasten/P. De Carli
    ATTN: G. Abrahamson
  4 cy ATTN: Y. Gupta
  4 cy ATTN: D. Keough
  4 cy ATTN: G. Duvall

Systems, Science & Software, Inc
    ATTN: Library
    ATTN: D. Grine

Terra Tek, Inc
    ATTN: S. Green

TRW Defense & Space Sys Group
    ATTN: Tech Info Cntr
  2 cy ATTN: N. Lipner

TRW Defense & Space Sys Group
    ATTN: E. Wong
    ATTN: P. Dai

Weidlinger Assoc, Consulting Engineers
    ATTN: M. Baron

Weidlinger Assoc, Consulting Engineers
    ATTN: J. Isenberg